A New Tool for Rock Mass Discontinuity Mapping from Digital Images: VTtrace

Alfred Vinod Antony

Thesis submitted to the faculty of the Virginia Polytechnic Institute and State University
in partial fulfillment of the requirements for the degree of

Master of Science
In
Civil Engineering

Dr. Joseph E. Dove
Dr. Marte S. Gutierrez
Dr. Matthew Mauldon

25 April 2005
Blacksburg, Virginia.

Keywords: Automated Fracture Mapping, Rock Mass Characterization, Digital Imaging, Digital Image Processing

Rock Mass Discontinuity Trace Detection Using VTtrace

Alfred Vinod Antony

ABSTRACT

Manual fracture mapping in tunnels, caverns, mines or other underground spaces is a time intensive and sometimes dangerous process. A system that can automate this task could minimize human exposure to rockfalls, rockbursts or instabilities and facilitate the use of new methods of data visualization such as virtual environments. This research was undertaken to develop VTtrace; a semi-automatic fracture mapping algorithm based on image processing and analysis techniques. Images of a rock exposure surface are made using a "prosumer" grade digital camera. The grayscale images are preprocessed to remove color information and any noise or distortion. The smoothed images are converted into binary images. The binary images are then thinned to extract the fracture map. The fractures are then separated and stored as different images. Fracture properties such as the length, width, orientation and large-scale roughness are determined using photogrammetric techniques. Results from test images shows the VTtrace is effective in extracting rock discontinuity traces. Additional enhancements to the program are proposed to allow feature attributes from the three-dimensional surface to be determined.

Acknowledgements

The author wishes to express his ultimate gratitude to the Almighty for giving an opportunity to work and complete this research.

The author presents a bouquet of thanks and appreciation to his advisor, Dr. Joseph E. Dove, for his guidance, encouragement, and support throughout the research and for the intensive review of the thesis.

The author is also grateful to:

Dr. Marte S. Gutierrez, for giving him the opportunity to work on this research project and for his kind cooperation and support during the research.

Dr. Matthew Mauldon for his guidance and advice.

His wife, Veena Jose for her love, support and encouragement.

His associates, Jeramy Decker, Sotirios Vardakos and Imsoo Lee for their support and friendship.

A special thanks to National Science Foundation for funding this research project.

Finally, the author expresses his sincere thanks to Virginia Tech for providing all the facilities, infrastructure and research friendly environment.

Table of Contents

List of Figures

Chapter 1 Introduction

Accurately recording the distribution, pattern and attributes of rock mass discontinuities is an important problem in geoengineering. Fractures, joints and faults largely control the engineering behavior of rock masses and their intersections can create deadly rockfall hazards. In addition, there is a need within the geoengineering community for tools that will allow better storage, retrieval, visualization and use of discontinuity information.

This thesis presents the research undertaken to develop VTtrace, a semi-automatic program for rock mass discontinuity trace detection using digital image processing and analysis techniques. The research is a part of the overall research and development effort for the project "Adaptive Real-Time Geologic Mapping Analysis and Design of Underground Space" (AMADEUS) supported by the National Science Foundation.

This chapter highlights the importance of this research, motivation for accomplishing the work and the problems for which it is intended to solve. A brief overview of the methodology used is also provided.

1.1 Motivation & Objective

Manually mapping discontinuities on the faces of rock exposures is a time intensive and sometimes dangerous process. Mapping requires that the geoengineer or geologist be directly adjacent to a rock face and in the zone of influence for events such as rock falls, rockbursts or other instabilities. Moreover manual measurements are confined to the area of reach and thus may not be an accurate representation of the entire surface. There is also a limitation on the amount of data that can be collected manually due to time and budget constraints.

By extracting traces and attributes of rock discontinuities from images of the same rock face made at a safe distance, there will be benefits in terms of safety and productivity. Digital segmentation and storage of discontinuities and attributes will also facilitate the use of new methods of data visualization, such as virtual environments. Therefore such a system has great practical significance to the geoengineering profession and society at large.

The objective of this research effort is to develop a semi-automated system to extract discontinuity traces on rock surfaces using digital processing and analysis techniques. The system is able to estimate fracture properties such as the length, width, roughness and orientation.

1.2 Terminology

The term discontinuity as applied to a rock mass refers to faults, joints, fractures and bedding planes that form abrupt structural boundaries. A joint is a break in the rock mass, which has not had any noticeable movement or displacement. A fault is a break in the rock mass that has had noticeable movement or displacement along the break. A bedding plane is the surface parallel to the surface of deposition (Reid 1998). Bedding planes are features of sedimentary rocks.

The act of creating a digital representation of a rock mass is referred to as imaging. An image is the actual digital representation that is available on a storage medium. Image processing involves sequentially modifying the original image using various mathematical filters. Much of the work described in this thesis involves image processing. Image analysis is the quantitative measurement and/or estimation of parameters or features in the image.

1.3 Application of Digital Image Processing and Analysis Techniques

Digital image processing has been used since early 1920's. In the 1960's with the arrival of digital computers, there was rapid advancement in the algorithms and methodologies for image processing and analysis. Image processing techniques found application in various fields like industrial inspection, biomedical engineering, remote sensing, optical character recognition, metrology and photogrammetry, aid for people with disabilities and many more. The application of image processing techniques in rock mechanics has been an area of active research as described in the next chapter.

1.4 Organization and structure

This thesis is divided into six chapters. Chapter 2 examines the literature on previous work on automated discontinuity trace detection. The literature review is also compared with this research and the similarities and the uniqueness of this research is

presented. Chapter 3 gives an introduction to the image processing and analysis concept. Fundamental concepts of the image processing techniques used in this research such as thresholding, smoothing, thinning and edge detection are explained in detail. Chapter 4 presents the new methodology for the semi-automated detection of discontinuity traces using digital images. The proposed imaging system and the algorithm for each process is outlined. Chapter 5 provides the test cases and results for the new system with different rock mass images and varying user selected parameters. Conclusions are drawn as to the success and accuracy of the system. Chapter 6 states the practical problems and challenges that could be encountered while implementing this system and lists recommendations for future research.

Chapter 2 Review of Previous Related Research

The use of digital imaging, image processing and photogrammetry methods as tools for geological and geomechanical rock characterization is a developing area of research. Enabling technologies for developing this tool come from the fields of computer science and geoengineering. By fusing technologies from the fields, methods of characterization can be developed that add to value and quality of project engineering. This chapter documents previous research results that were found to the most relevant for developing a semiautomatic fracture mapping tool.

Several studies have been published regarding fracture mapping and rock mass characterization of rock surfaces using digital images. Lemy and Hadjigeorgiou (2003) demonstrated the advantages and use of image analysis techniques for rock mass characterization. Their approach to this problem was to construct the discontinuity trace maps with the aid of artificial neural networks. The superfluous segments of the trace map that do not constitute the discontinuity trace are recognized by the neural network algorithm and are removed. The final step is to identify and connect segments delineating the same trace. This is achieved by linking all the recognized segments into a continuous line representing a discontinuity trace.

Rock mass characterization parameters like the Rock Quality Description (RQD), discontinuity trace length and discontinuity frequency are determined by implementing photogrammetric techniques, where a digital elevation map of the rock surface is created. The neural network algorithm used in this research requires a training database that contains features expected in the actual images. It was found that the algorithm could not recognize all features in images, which then required human intervention to complete the trace map. The use of neural networks for the current research was determined to be cumbersome with little added value at this time. In addition VTtrace is not intended to be a fully automatic mapping system, as it is believed that human input is needed. However, neural networks might possibly be the best solution for developing automatic systems.

Reid and Harrison (2000) presented a methodology for semi-automatic detection of discontinuity traces in grayscale digital images of rock mass exposures. This methodology detects discontinuity traces as individual objects, and by doing so distinguishes one discontinuity trace from another. Discontinuity trace detection is achieved by using the concept of 'topographic feature labeling', developed by Reid (1998), and through the development of a method to link together the curvilinear features in digital images of rock mass exposures. The basic requirement for the discontinuity trace is that it must have a different brightness from the intact rock surface. It is evident that a change in pixel value occurs as a discontinuity is crossed. On either side of the discontinuity, pixel values change in a continuous manner until the minimum pixel value is reached. If pixel values are envisioned as a continuous surface, the minimum pixel values would be located in "ravines".

By calculating the first and second derivatives, the curvature of a plane normal to the surface is obtained. As the plane is rotated about the surface normal to itself, the curvature varies (provided that the surface is neither planar nor spherical). When the curvature becomes either a maximum or a minimum it is called principal curvature, and the directions in which this occurs are called principal axes of curvature. These principal directions are represented by the eigenvectors of a symmetric matrix and are therefore mutually orthogonal. The local shape of the surface is established by considering the first and second derivatives of the plane curve in the directions of maximum curvature. A point on a surface can be assigned a topographic label, such as ravine, ridge, peak or pit

The most important aspect of the Reid and Harrison approach is the separation of the line segments into different objects. This is accomplished by identifying the ravine pixels, tracing the line segments formed by connecting the ravine pixels and then labeling the ravine line segments. A linking algorithm is used to connect gaps in the fracture traces. However, the selection of end pixels that has to be linked with to another pixel has to be done manually. Manual selection of the end pixel will become very tedious for some cases especially when there are many images to be processed. To make this method truly automatic, an algorithm to connect the loose ends of the line segments is required.

Kemeny et al. (2003) studied the use of Digital Imaging combined with laser scanning technologies for field fracture characterization. This method has been developed into a commercial software package called “Split FX” marketed by Split Engineering, Inc. The program is able to use digital images or 3-D laser scanning information. It can delineate fracture traces, determine joint sets, provide 3-D orientation information for joints and can perform block analysis.

The fracture traces are delineated from the digital images using a modified Hough transform. Fractures are then separated into sets using an algorithm developed specifically for this purpose. Once the fracture sets have been identified, several kinds of information are determined for each fracture set. The most important is the extraction of 3D orientation from the fracture trace information. 3D fracture information is obtained with the information acquired from two or more non-parallel faces.

The second method suggested by the authors is to use Lidar laser scanning technology to acquire the digital elevation map of the field surface. The laser scanner gives a point cloud from which specific information about the fractures in the rock mass such as orientation, density, size, spacing, roughness etc. are determined. The digital images used for the analysis of traces should be taken with the camera set up perpendicular to the rock wall. Correction for inclined camera view is not incorporated in this system. The orientations of the fractures can also be calculated using image processing and photogrammetry techniques. The use of laser scanning technology for fracture traces is a great advancement but there are concerns over the efficiency of the laser scanner on wet surfaces and the time required for processing the point clouds. The laser scanner gives a 3D point cloud from which the trace maps and the 3D mesh is developed using a statistical model.

It is not possible from the literature published on Split FX to determine how well the components function and the areas of development are required. It does seem to yield those parameters and information that are most important to geomechanical characterization.

Gaich et al. (http://www.ifb.tugraz.at/situ/) developed an "Electronic Imaging System" to capture high-resolution stereoscopic image for tunnel construction. The

system uses calibrated rotating color line scan cameras and photogrammetric orientation principles for 3D site measurements. The system uses images from on-site mapping. Each image represents a surface area of about 10 m width and 8 m in height. Features, such as fractures, in the range of a few centimeters can be resolved.

The imaging system consists of two digital CCD-line sensor cameras with 6000 elements mounted on rotating camera heads. These are fixed with a rigid frame on a vehicle. Rotation of the cameras projects panoramic images onto a cylindrical surface. This imaging technique and the correct seaming of single image parts is used within the various components of the application.

The interior orientation of the cameras and the geometry of the imaging set-up are calibrated in the laboratory. Rigid transformations between the cameras and a world respective tunnel co-ordinate system are also set. The 3D measurement and reconstruction is based on the epipolar principal. From the known interior and exterior orientation of the cameras and the calculation of the corresponding picture points the object point is reconstructed. The analysis results in a triangulated irregular network (TIN) map.

Accuracy of the 3D reconstruction depends on proper laboratory calibration of cameras and imaging set-up in the field, co-ordinates of the geotechnical convergence marks used for computing the exterior camera orientation being precisely determined, resolution of the images, image quality, and localization of corresponding points in the stereo images (automatic and interactive).

An interactive program called GeoEDIT was developed for geomechanical characterization. It allows the geologist to evaluate structural features of tunnel face images. Traces of discontinuities, boundaries between different lithologies etc. can be identified with this tool. To distinguish between different structures in an image, grouping by a layer concept is adopted and displayed in different colors. Visualization of the tunnel face can be accomplished by using shutter glasses.

Soole and Poropat (2000) applied photogrammetry methods to highwall mapping, visualization and landslide assessment. The terrestrial photogrammetry system is targeted at data collection and mapping requirements for highwall mapping, general

mine site documentation and validation and interpretation of mine data. The system developed by the authors has simple field procedures, is capable of making direct measurements of position in orientation parameters using an integrated GPS, orientation sensors and digital camera hardware for quick data capture and has easy to use digital photogrammetry software.

Using the data and digital image of a rock mass a separate commercial program (SIROJOINT) is used to identify, map, annotate and analyze visible structural features. With this program, the user can identify and measure the orientation, area and position of joint faces and joint traces; identify and measure geological features such as bedding planes, faults etc.; identify dominant joint sets using contoured stereonets of orientation vectors; classify joints according to orientation; calculate spacing for joint sets and bedding planes and annotate joints with termination information.

Based on the above previous research, the following points are made regarding development of VTtrace:

- A practical and easy to use fully automatic detection system may not be possible at this time. Semiautomatic methods may offer more flexibility for the geologist or engineer in selection and representation of discontinuities but at a higher time price.
- Either line scan or prosumer digital cameras are suitable for image collection. Lidar systems can also be used but are expensive at the present.
- A system that uses 'off-the-shelf' technology has the potential for greater acceptance in the geoengineering community.

Chapter 3 Overview of Imaging and Image Processing

This chapter provides the reader with a brief overview of how images are created and acquired, and a discussion of basic image processing methods. There are numerous books and papers available on this topic. Technologies for image processing are largely from the computer science and electrical engineering fields; however, they are used in many crosscutting applications.

3.1 Early Cameras and Image Formation

The first cameras were known as "pinhole cameras". Essentially this was a box with a small hole in one of its sides, and a photographic plate on the opposite side. Rays of light travel in straight lines from the 3D scene onto the photographic plate Forsyth et al. (2003). The working of a pinhole camera is schematically illustrated in Figure 3.1

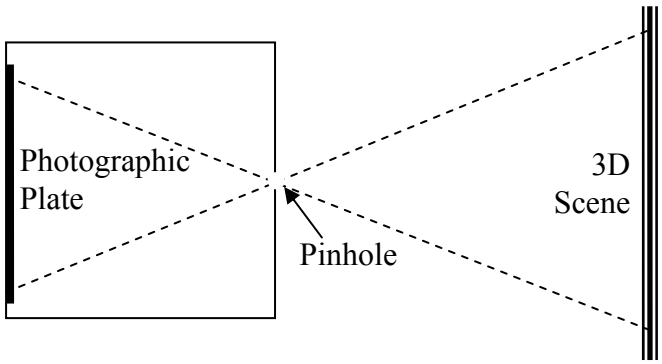

Figure 3.1. Illustration of a pinhole camera.

The image in a pinhole camera is formed by light rays that issue from the scene facing the box. The image is formed by the principle of perspective projection, also known as "pinhole perspective or "central perspective" projection model (Forsyth et al. 2003). Perspective projection model is illustrated in Figure 3.2. Perspective projection creates inverted images.

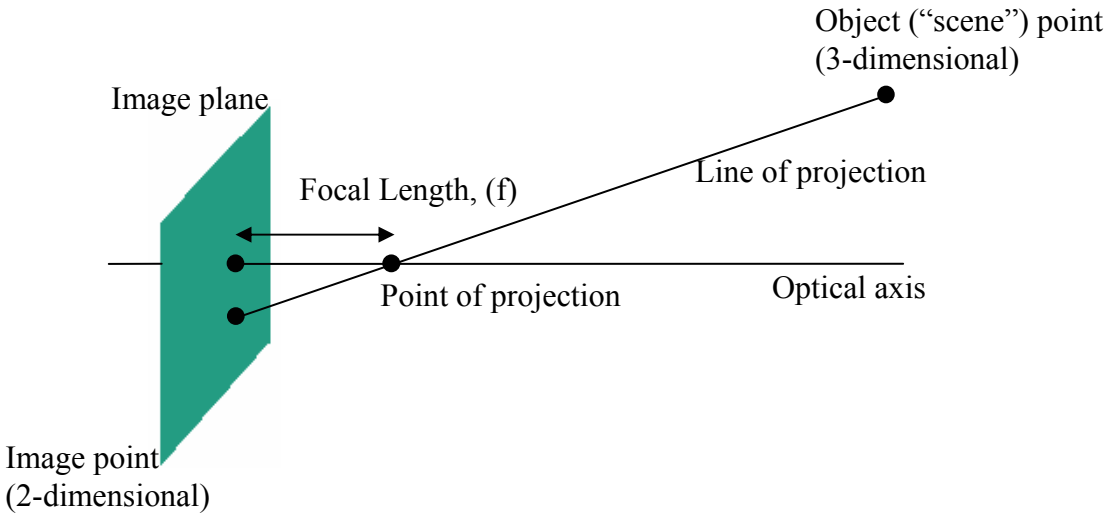

Figure 3.2. Illustration of the Perspective Projection model.

3.1.1 Cameras with Lenses

There are two major reasons why cameras are equipped with lenses. First, lenses are used to gather more light than just a single ray as in the pinhole camera. Real pinholes have a finite size, so each point in the image plane is illuminated by a cone of light rays subtending a finite solid angle. The larger the hole, the wider the cone and the brighter the image. However, a larger pinhole produces a blurry image. Shrinking the pinhole produces sharper images but reduces the amount of light reaching the image plane and may introduce diffraction effects Forsyth et al. (2003).

The second main reason for using the lens is to keep the picture in sharp focus while gathering the light from the object. Therefore, the problem with pinhole size is eliminated.

3.1.2 Digital Cameras

A digital camera is similar to a conventional camera in that it has a series of lenses that focus light to create an image of an object. But instead of focusing the image light onto a photo-chromatic film, an electronic sensor is used that converts light to electrical charges. The image sensor employed by most digital cameras is a charge coupled device (CCD). A CCD sensor uses a rectangular grid of electron-collection sites laid over a thin silicon wafer to record a measure of the amount of energy reaching each of them. Each site is formed by growing a layer of silicon dioxide on the wafer and then

depositing a conductive gate structure over the dioxide. When light photons strike the silicon, electron-hole pairs are generated (photo-conversion), and the electrons are captured by the potential well formed by applying a positive electrical potential to the corresponding gate. The electrons generated at each site are collected over a fixed period of time.

The charges stored at the individual sites are moved using charge coupling where charge packets are transferred from site to site by manipulating 'gate potentials' that preserve the separation of the packets. The image is read out of the CCD one row at a time, each row being transferred to a serial output register with one element in each column. Between two row reads, the register transfers its charges one at a time to an output amplifier that generates a signal proportional to the charge it receives. This process continues until the entire image has been read out. It can be repeated 30 times per second for video applications or at a much slower pace, leaving ample time for electron collection in low light level applications such as astronomy. The digital output of most CCD cameras is transformed internally into an analog video signal before being passed to a frame grabber that constructs the final digital image.

3.1.3 Image Representation

A digital image is a 2-dimensional array of intensity values. Each element in the array in known as “pixel” (picture element). The position of each element in the array represents spatial co-ordinates in the scene, and the value of each cell represents the pixel intensity values or brightness value. Common image sizes are 480 pixels (rows) by 640 pixels (columns) and 512 pixels by 512 pixels. The resolution of the digital image is related to the physical size of the sensor array within the camera, which is usually specified in terms of the horizontal and vertical pixels or may be specified as the total number of pixels.

A histogram is a representation of the distribution of observed pixel values. For an image, the histogram indicates the number of pixels having a particular value. The histogram of an image *h(i)* can be represented as follows:

$$h(i) = \frac{1}{N} \sum_{r} \sum_{c} p(r, c, i), \tag{3.1}$$

$$\text{where } p(r,c,i) = \begin{cases} 1 & \textit{if pixel value at } (r,c) = i \\ 0 & \textit{otherwise} \end{cases}$$

$$N = \text{Number of pixels.}$$

Usually the division by N is omitted for convenience. Histogram is often used as an estimate of the probability distribution of image intensities. It does not contain the information of the position of the pixels. It is commonly assumed to have a Gaussian distribution. Histogram analysis is used in various image processing operations like thresholding, edge detection etc. An example of an image histogram is shown in Figure 3.3.

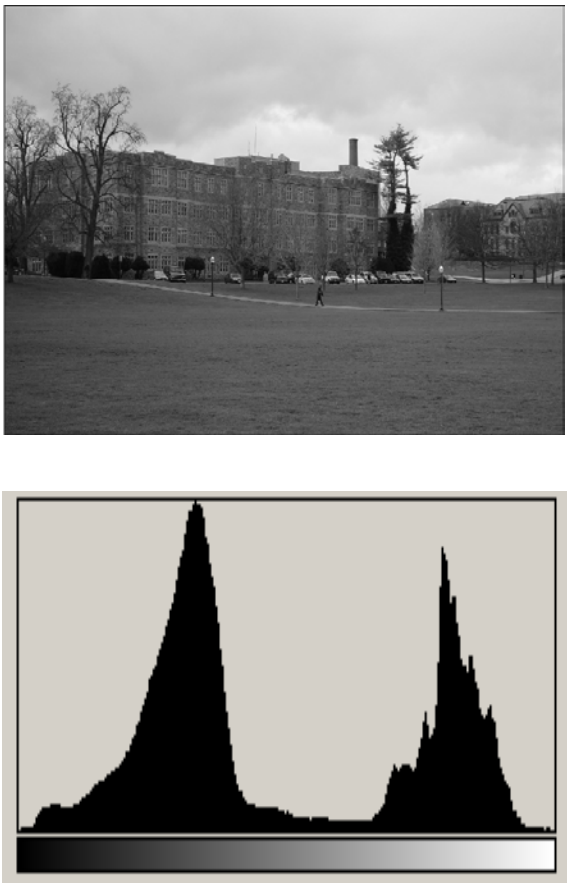

Figure 3.3. A grayscale image and its histogram.

3.2 Image Processing Operations

Image processing techniques are applied in various fields such as pattern matching, quality control in an assembly, special effects, and automated tracking. More recently image processing techniques have been developed for rock mass fracture trace mapping. Image processing is conduced in stages and some of most common stages are explained below.

3.2.1 Smoothing

Images typically have the property that the value of a pixel is usually similar to that of its neighbor. If the image is affected by noise in the form of dead pixels or other defects the effects of noise is reduced by replacing the pixel value by the weighted average value of its neighbors. This process is known as smoothing, blurring or noise reduction. Various filters can be used to perform this operation. Some of the common filters, known as box or linear filters, are shown in Figure 3.4

$$\begin{bmatrix} 1 & 1 & 1 \\ 1 & 1 & 1 \\ 1 & 1 & 1 \end{bmatrix} \bullet \frac{1}{9} \qquad \begin{bmatrix} 1 & 4 & 1 \\ 4 & 8 & 4 \\ 1 & 4 & 1 \end{bmatrix} \bullet \frac{1}{28}$$

$$\begin{bmatrix} 1 & 1 & 1 & 1 & 1 \\ 1 & 1 & 1 & 1 & 1 \\ 1 & 1 & 1 & 1 & 1 \\ 1 & 1 & 1 & 1 & 1 \\ 1 & 1 & 1 & 1 & 1 \end{bmatrix} \bullet \frac{1}{25}$$

Figure 3.4. Various box filters.

These filters are very popular because of their simplicity. The effect of 5X5 smoothing filter is shown in Figure 3.5.

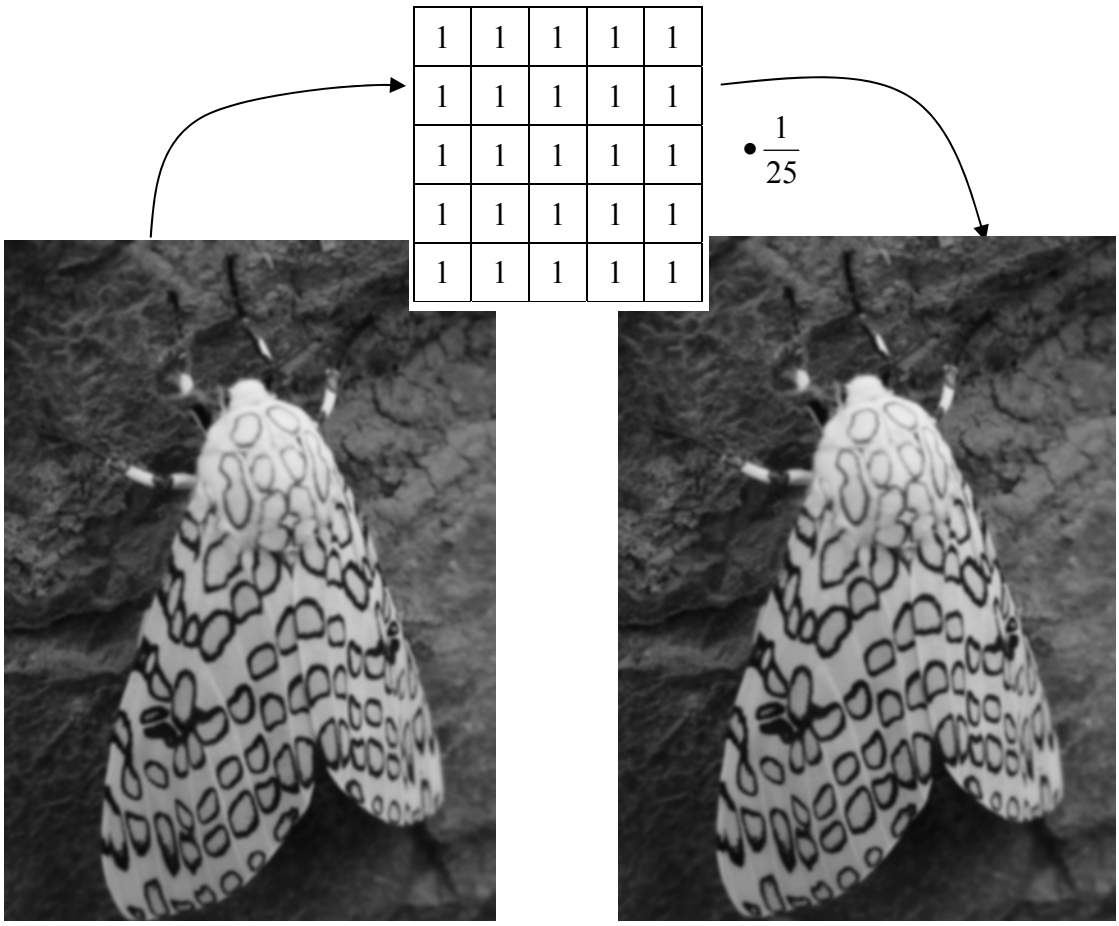

Figure 3.5. Result of the 5X5 Linear smoothing operation.

3.2.2 Thresholding

Thresholding is the process of converting a gray scale image to binary image. A binary image is an image in which there can be only two possible pixel values. These are called the "foreground" and the "background" values. Usually the foreground is black (value = 1) and background is white (value = 0). The simplest way to make this conversion is to compare each pixel value in the gray scale image to a fixed threshold value. If the pixel value is less than the threshold value, then the pixel is assigned to the foreground and if it is greater than the threshold assign it to background, or vice versa.

If T is the threshold value then:

$$I_{NEW}(r,c)=\begin{cases}1 & if \quad I(r,c)\le T\\ \\ 0 & if \quad I(r,c)>T\end{cases}, \tag{3.2}$$

where I is pixel value and r and c refer to image matrix row and column, respectively. In some situations, the conditions may be reversed as follows:

$$I_{NEW}(r,c)=\begin{cases}1 & if \quad I(r,c)>T\\ \\ 0 & if \quad I(r,c)\le T.\end{cases} \tag{3.3}$$

Examples of images with different threshold values are shown in Figure 3.6.

Original Image T = 100 T = 128 T = 205

Figure 3.6. Examples of thresholding.

Picking the threshold value is critical, as it will determine the actual image used for subsequent analysis. A threshold level that captures the features critical to the application should be used. Possibly the best to ensure the desired image is to manually enter a threshold value for each image. However there are also automatic ways of picking the threshold value. One of the most popular methods is known as the "Otsu's Method" (Otsu 1969). Otsu's method assumes that the histogram of the grayscale image is bimodal with modes representing dark and light areas. The thresholding problem is to pick up the threshold value, T, separating the two modes of the histogram from each other. Each T

determines a variance for the group of values that are less than or equal to T and a variance for the group of values greater than T. The definition for the best threshold suggested by Otsu (1969) is that threshold for which the weighted sum of group variances is minimum. The weights are the probabilities of the respective groups. This method will be described in detail in following chapters.

3.2.3 Edge Detection

Points in the image where brightness changes rapidly are often called "edges" or "edge points". Many different edge detection methods have been developed over the years. Edge detection begins by plotting the intensity values of a single image row as shown in Figure 3.7. Change in the intensity values can be detected by estimating the first derivative of the image intensity. Since it is a single row, the problem is one-dimensional.

Let f(x) represent the intensity profile, the first derivative is given by:

$$\frac{\partial f}{dx} = \lim_{\Delta x \to 0} \frac{f(x+\Delta x) - f(x)}{\Delta x}, \tag{3.5}$$

and can be approximated as:

$$\frac{\partial f}{dx} = \frac{f(x+\Delta x) - f(x)}{\Delta x}. \tag{3.6}$$

For a two dimensional image array I(x,y) with a pixel distance of Δx, the derivatives can be estimated as follows:

$$\frac{\partial I}{dx} \approx \frac{f(x+\Delta x, y) - f(x,y)}{\Delta x}, \tag{3.7}$$

and

$$\frac{\partial I}{dy} \approx \frac{f(x, y+\Delta y) - f(x,y)}{\Delta y}. \tag{3.8}$$

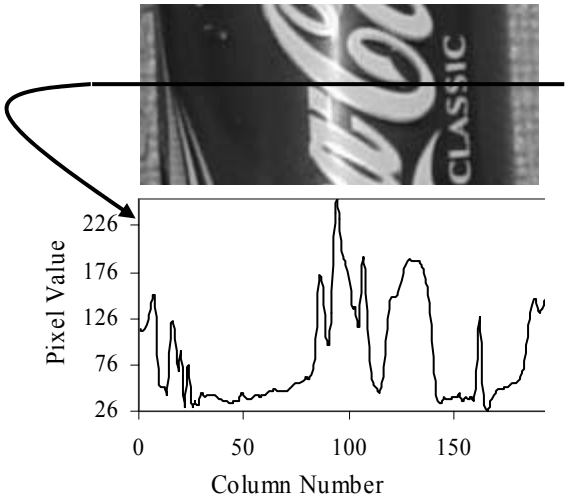

Figure 3.7. Intensity plot for a single row of pixels.

For discrete image array I(r,c), if Δx is the width of one pixel, the derivative can be expressed as follows:

$$\frac{\partial f}{dx} \approx \frac{I(x+\Delta x, y) - I(x,y)}{\Delta x} \longrightarrow I_x(r,c) = I(r,c+1) - I(r,c), \qquad (3.9)$$

where:

$I_x(r,c) = I(r,c+1) - I(r,c)$ can be written as $I_x(r,c) = I(r,c)\cdot -1 + I(r,c+1)\cdot 1$. This latter term can be used as the 'mask' for Equation 3.9 and can be rewritten in matrix notation as: [-1 1].

During the edge detection operation, the mask is moved over the original image and a new image is created. This process is illustrated in Figure 3.9.

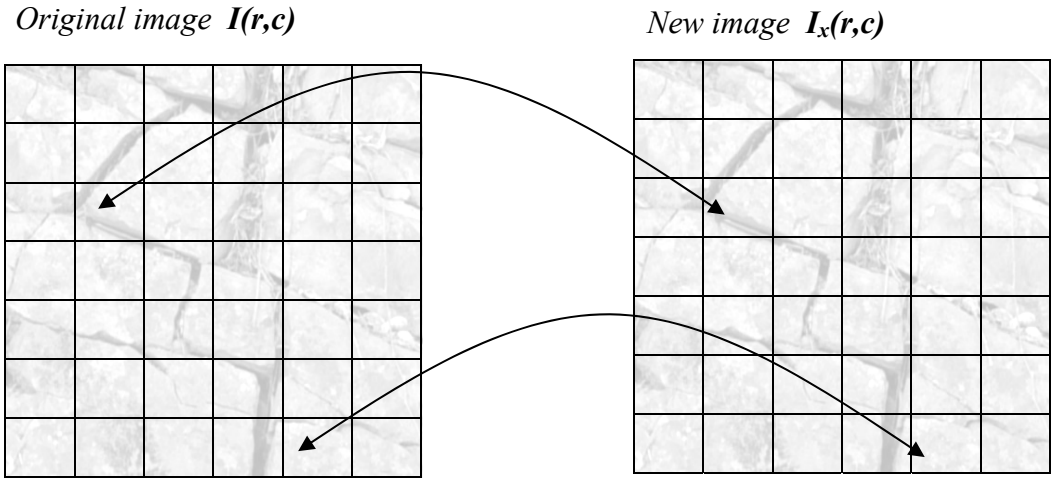

Figure 3.8. Illustration of the edge detection operation.

Some commonly used edge detection filters include:

Sobel Operator

-1	0	1
-2	0	2
-1	0	1

Prewitt

-1	0	1
-1	0	1
-1	0	1

Roberts

1	0
0	-1

Some of the advanced non linear edge detectors are the Gaussian operator, Laplacian of Gaussian (LoG), Canny edge detectors.

3.2.4 Thinning

For a wide rock discontinuity, the width of the image element is greater than one pixel. It is convenient to reduce the width so that subsequent operations are easier and more accurate. Thinning is the process of reducing the width of an image element to just a single pixel. The process erases the black pixels such that an object without holes erodes to minimally connected stroke located equidistance from its nearest boundaries (Pitas 2000). Minimally connected means that adjacent black pixels share common corner or side. No single pixel has more than two neighboring pixels. Standard thinning algorithms proposed by Zhang et al. (1999) and Hildtich (1969) are explained in detail in the following chapter.

A skeleton or stick figure representation of an object is often used to describe its structure (Pitas 2000). Sometimes the outcomes of thinning and skeletoning will be unique but it is not always the case.

Chapter 4 Detection of Rock Mass Discontinuity Traces

The digital image processing techniques explained in the previous chapter can be used to generate rock mass discontinuity trace maps. A description of the methodology and algorithms used in VTtrace are described in this chapter. In the present program, the length, width, roughness and orientation of the discontinuities in the two-dimensional image plane are determined from the traces. Continuing work will employ photogrammetry techniques to determine the fracture attributes such as the true length, width, roughness and orientation of the discontinuity plane.

The sequence of steps adopted to generate the discontinuity trace map is show in the flow diagram in Figure 4.1.

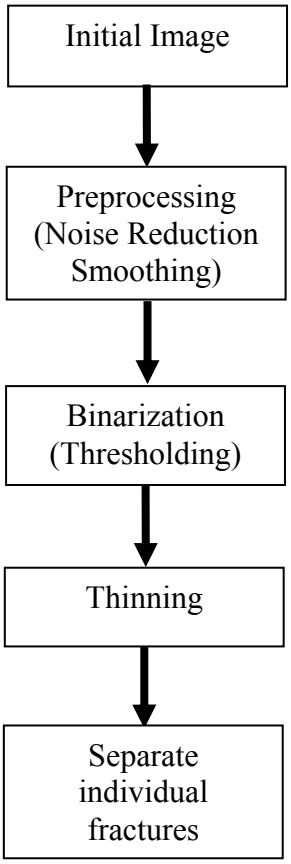

Figure 4.1 Sequence of processes to extract the fracture trace map.

4.1 Imaging Acquisition and Equipment

A schematic diagram showing the configuration of the final imaging system is shown in Figure 4.2. The system will have two digital cameras, a laser distance meter and a target projector all mounted on a rigid bar capable of rotating the equipment through a vertical arc of 180 degrees. A portable computer will be used for image acquisition, control of the cameras and initial image processing. Currently, for this first portion of the project, a single "prosumer" grade Nikon D-100 digital camera with a resolution of up to 6.1 megapixels mounted on a conventional tripod is used to capture images. This camera uses an 18 – 35mm wide angle lens. In the final system, it is envisioned that images will made to overlap for stereo matching.

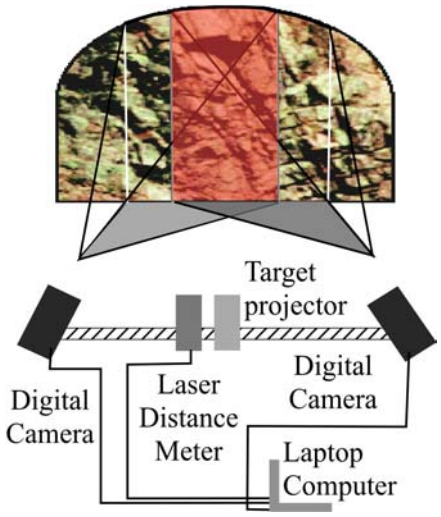

Figure 4.2. AMADEUS rock mass imaging system.

4.2 Image Processing Overview

The captured digital image of a fractured rock mass is converted to a grayscale image by removal of the color information. The grayscale image is first preprocessed to remove noise and distortion by the process of smoothing. An algorithm is then used to threshold the image resulting in a binary image. A threshold value is selected such that pixels below the threshold value are converted to black and all the pixels above the threshold value are converted to white. The binary image will have only black or white pixels. The binary image is then thinned to extract the fracture maps. Capabilities are

provided so that the fracture maps can be edited and annotated manually with the help of drawing tools, such as a pencil and an eraser, to remove any unnecessary lines. The individual fractures on the edited image are then separated from the fracture map and saved as separate image files. Lastly, the individual fracture attributes like the length, width, orientation and large scale roughness are determined. Each stage of image processing is explained in detail in the following paragraphs.

4.2.1 Smoothing

This is the first step of the image processing stage. A non-linear low pass smoothing filter such as the median filter was implemented to reduce the noise in the image. Non-linear filters were used since they are very effective and preserve the image edges and details. The median filter not only smoothes noise in homogenous image regions but tends to produce regions of constant or nearly constant intensity.

The two-dimensional median filter is defined as:

$$y(i,j) = med\left\{x(i+r, j+s), (r,s) \in A, (i,j) \in Z^2\right\}, \tag{4.1}$$

where $Z^2 = Z * Z$ denotes the rectangular digital image plane. The set $A \in Z^2$ defines the filter window. The border pixels are ignored.

To implement a median smoothing filter, the user must first specify a window size such as 3X3. Then, for each position of the window within the original image, the algorithm sorts the pixel values in order then computes the statistical median of those pixel values. This median value is the new pixel value on the output image. This process is illustrated on Figure 4.3.

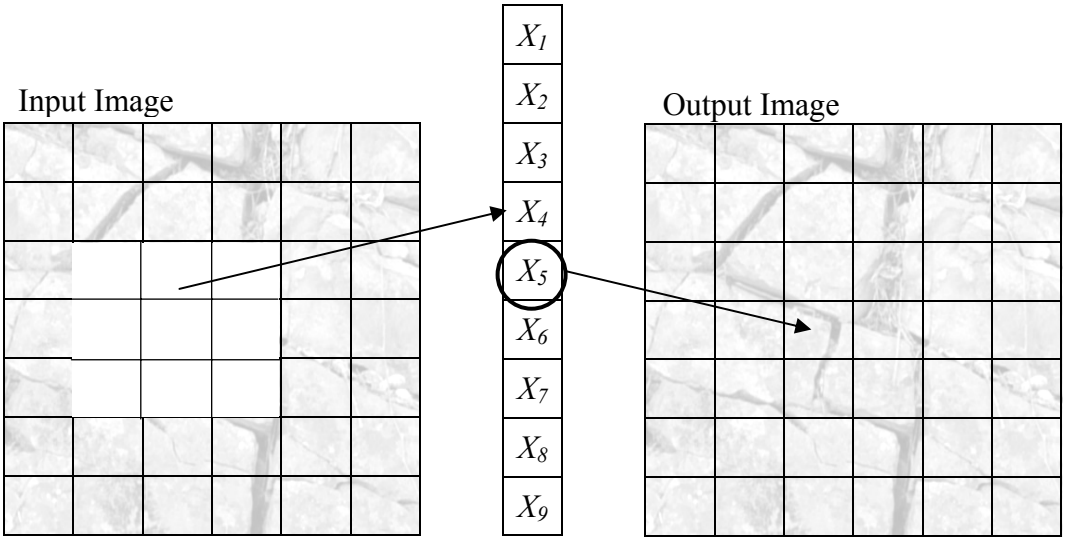

Figure 4.3. Illustration of a 3X3 window median filter. X4 is the median value of the 3X3 window and becomes the new value of the output image.

4.2.2 Thresholding

The smoothened image is converted to a binary image by the process of thresholding. A binary image is an image in which the pixels assume one of the two possible values. Usually the two values are know as "foreground" and "background" values.

The thresholding process compares every pixel with a given constant threshold value (T). If the pixel value is below the threshold, the pixel is changed into a foreground pixel. However, if the pixel value is above the threshold, it is changed into a background pixel.

The threshold value can be a user input or selected automatically using the distribution of image intensities. Automatic selection is accomplished by Otsu's method (Otsu 1969).

In this method it is assumed that the histogram is bimodal (i.e., there are two natural groups of intensity values). For each value of T, the variances of the two groups

are computed. The threshold value is the value of T for which the expected value of the group variance is minimum.

It can be mathematically expressed as follows:

$$q_1(t) = \sum_{i=0}^{t} h(i), \tag{4.2}$$

and

$$q_2(t) = \sum_{i=t+1}^{255} h(i). \tag{4.3}$$

The group variance, σ^2 (t), is written as:

$$\sigma_w^2(t) = q_1(t)\sigma_1^2(t) + q_2(t)\sigma_2^2(t). \tag{4.4}$$

4.2.3 Thinning

Thinning is used to obtain the fracture traces on the rock surface. Two thinning algorithms are included in the program and the user can opt for either. The first thinning algorithm is a sequential raster scanning algorithm also known as Hilditch algorithm, Hilditch (1969). The second method is a parallel algorithm developed by Zhang and Suen (1984). Each method is discussed below.

4.2.3.1 Hilditch's Algorithm

The Hilditch algorithm determines pixels for deletion from the image. Deletion in this case means transferring from an object pixel to background pixel based on the specified conditions described below. The algorithm traverses the image in a raster scanning sequence from top to bottom and left to right. After each raster scan the identified object points are transferred into background pixels. The algorithm stops when no pixels are found that fulfills the criteria.

A pixel is removed if it satisfies *all* of the following conditions:

Condition 1. It is a foreground pixel, where:

$$I(r,c) = 1. \tag{4.5}$$

Condition 2. It is located on the boundary. This is satisfied if at least one of its four neighbors belongs to the background or has been removed from the

foreground pixels. A pixel is considered to be on the background at the end of the iteration. Figure 4.4 shows four possible arrangements of pixels, where P is the pixel currently being considered by the algorithm.

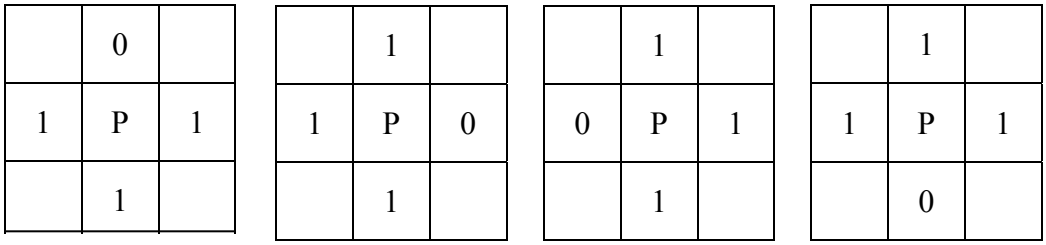

Figure 4.4. Four possible arrangements of pixels.

The numbering sequence of the pixels is shown in Figure 4.5. The algorithm in this step computes the value of the function $f_1(p) = a_1 + a_3 + a_5 + a_7$. If the pixel value at $n_i = 1$ (foreground), then $a_i = 0$, otherwise $a_i = 1$. If $f_1(p) \geq 1$ then the pixel P will be changed to background (value = 0).

n_4	n_3	n_2
n_5	P	n_1
n_6	n_7	n_8

Figure 4.5. Numbering sequence of the neighborhood pixels.

Condition 3. It is not at the end of a thin line. This requires that at least two of its eight neighbors not belong to the background nor have been removed from the foreground pixels. This is determined as follows:

$f_2(p) = \sum_{i=1}^{8} b_i$, where $b_i = 1$ if $I(r,c) = 1$ and $b_i = 0$ otherwise.

If $f_2(p) \geq 2$, then the pixel P will be changed to background. (4.7)

Condition 4. It is not an isolated point, (at least one of its eight neighbors is a foreground pixel).

$$f_3(p) = \sum_{i=1}^{8} b_i ,$$

where $b_i = 1$ if $I(r,c) = 1$ and $b_i = 0$ otherwise, and

$$f_3(p) \geq 1. \tag{4.8}$$

Condition 5. If the removal of a pixel does not alter connectivity of the foreground pixels. The number of connected components in the eight neighbor region is determined using the Hilditch's crossing number. The Hilditch's crossing number of a pixel is calculated by determining how many neighbors belong to the background (value =0) and has either one of their next two neighbors in the eight-neighborhood region that is a foreground pixel or have been removed.

$f_4(p) = X_H(p) = \sum_{i=1}^{4} c_i$, where $c_i = 1$ if $f(n_{2i-1}) = 0$ and either $|f(n_{2i})| > 0$

or $|f(n_{2i+1})| > 0$, $c_i = 0$ otherwise) and,

$$f_5(p) = 1. \tag{4.9}$$

The calculation of Hilditch's crossing number is further illustrated in the following example shown in Figure 4.6.

0	*1*	*0*
1	*p*	*1*
0	*1*	*0*

(a) Crossing Number $X_H(P) = 0$

1	*0*	*1*
0	*p*	*0*
1	*0*	*1*

(b) Crossing Number $X_H(P) = 4$

Figure 4.6. Example of Hilditch's crossing number calculation.

In the above example, though both the cases have four foreground pixels, the crossing number is a minimum for one and a maximum for the other. In the example on

the left, each of the four adjacent neighbors are black pixels. In the example on the right, the four diagonal neighbors, n_2, n_4, n_6 and n_8,of the 8-neighbor region are black pixels.

4.2.3.2 Parallel Algorithm

The second thinning algorithm provided in this application is a parallel algorithm by Zhang and Suen (1984). This algorithm removes identified pixels from the foreground region except those points that belong to the skeleton. Each iteration consists of two sub-iterations also referred to as 'sub-cycles'. The first sub-iteration identifies the pixels to be removed that are located on the south-east boundary and the north-west corners. The second sub-iteration identifies the pixels to be removed that are located on the north-west boundary and the south-east corners. Both the sub-iterations are necessary to preserve the connectivity of the original regions on its skeleton because identified points are transferred in parallel. The thinning process terminates when no additional points are identified for deletion by both sub-iterations.

First Sub-Iteration. Each pixel in the image is examined and is deleted if it satisfies *all* of the following conditions:

Condition 1. The pixel belongs to the foreground region (pixel value = 1).

$$f_1(p) = 1 \tag{4.10}$$

Condition 2. It is a pixel identified for deletion but not an isolated point or the end of a thin line. The number of 8-neighbors that belong to the foreground region, is greater than or equals to two, and less than or equals to six.

$$f_2(p) = \sum_{i=1}^{8} n_i, \text{ where } 2 \le f_2(p) \le 6 \tag{4.11}$$

Condition 3. The number of white pixels located before a black pixel within its 8-neighbor region being equal to one. The 8-neighbors are ordered in the following sequence: n_3, n_2, n_1, n_8, n_7, n_6, n_5 and n_4.

Equation 4.11 is calculated by counting the number of transitions from a pixel on the foreground region to a pixel on the background and vice versa when traversing its 8-neighbors in anti-clockwise direction. It can only be an even integer, because transitions

must occur in pairs. If there is a transition between two pixels, there must be another transition associated with it. The valid crossing number in this case is 2.

$$f_3(p) = X_R(p) = \sum_{i=1}^{8} |n_{i+1} - n_i| \,, f_3(p) = 2 \,. \tag{4.12}$$

Figure 4.7 and Figure 4.8 shows examples of different pixel configurations and their crossing numbers.

1	*1*	*1*
1	*p*	*1*
1	*1*	*1*

(a) Crossing Number $X_H(P) = 0$

n_4	n_3	n_2
n_5	p	n_1
n_6	n_7	n_8

1	*0*	*1*
0	*p*	*0*
1	*0*	*1*

(b) Crossing Number $X_H(P) = 8$

Figure 4.7. Examples of pixel configurations for extreme cases.

Figure 4.7 illustrates two extreme cases where one has the minimum crossing number of zero and the other has the maximum crossing number of eight. In Figure 4.7 (a), all the eight neighbors are foreground pixels and in Figure 4.7 (b), the four diagonal neighbors, i.e., n_2, n_4, n_6 and n_8 are foreground pixels. The algorithm is not expected to encounter the example on the left, because it does not satisfy Condition 2.

1	*1*	*1*
1	*p*	*1*
0	*0*	*0*

(a) Crossing Number $X_H(P)$ =2

1	*1*	*1*
0	*p*	*0*
1	*1*	*1*

(b) Crossing Number $X_H(P)$ = 4

1	*0*	*1*
0	*p*	*1*
1	*0*	*1*

(c) Crossing Number $X_H(P)$ = 6

Figure 4.8. Additional examples of pixel configuration for extreme cases.

The three examples shown in Figure 4.8 demonstrate the possible 8-neighbor configurations with different resulting crossing numbers of two, four and six.

Condition 4. Any one of the three adjacent neighbors, n_1, n_3 and n_7, of the eight neighbors belongs to the background.

$$f_4(p) = n_1 \times n_3 \times n_7$$

$$f_4(p) = 0 \tag{4.13}$$

Condition 5. Any one of the three adjacent neighbors, i.e., n_1, n_7 and n_5 of the eight neighbors belongs to the background.

$$f_5(p) = n_1 \times n_7 \times n_5$$

$$f_5(p) = 0 \tag{4.14}$$

The second sub-iteration has the same conditions as the first sub-iteration, except for Conditions 4 and 5, which are replaced by their 180^o rotations. Condition 4 and 5 for the second sub-iteration are as follows:

4a. Any one of the three adjacent neighbors, n_5, n_7 and n_3, belongs to the background.

$$f_4(p) = n_5 \times n_7 \times n_3$$

$$f_4(p) = 0 \tag{4.15}$$

5a. Any one of the three adjacent neighbors, n_5, n_3 and n_1, belongs to the background.

$$f_5(p) = n_5 \times n_3 \times n_1$$

$$f_5(p) = 0 \tag{4.16}$$

The parallel algorithm stores the coordinates of all the points that satisfy all of the conditions above and those points are transferred into background points at the end of each sub-iteration.

4.2.4 Fracture Separation

After the fracture trace map is extracted, the individual fracture traces are separated and are saved as different image files. The starting point and the ending point of the individual traces are determined by the following conditions.

1. Let *P* be the first foreground pixel encountered while performing raster scan.

2. If a node or junction is encountered then it is assumed that the endpoint of the fracture is reached. Few examples of a node are shown in Figure 4.9. A pixel is identified as a node if it has more than one foreground pixel in the neighborhood region represented by n_1, n_2, n_6, n_7 and n_8 as shown in Figure 4.10.

		n_2
	p	n_1
n_6	n_7	n_8

Figure 4.9. Neighborhood pixels while identifying nodes.

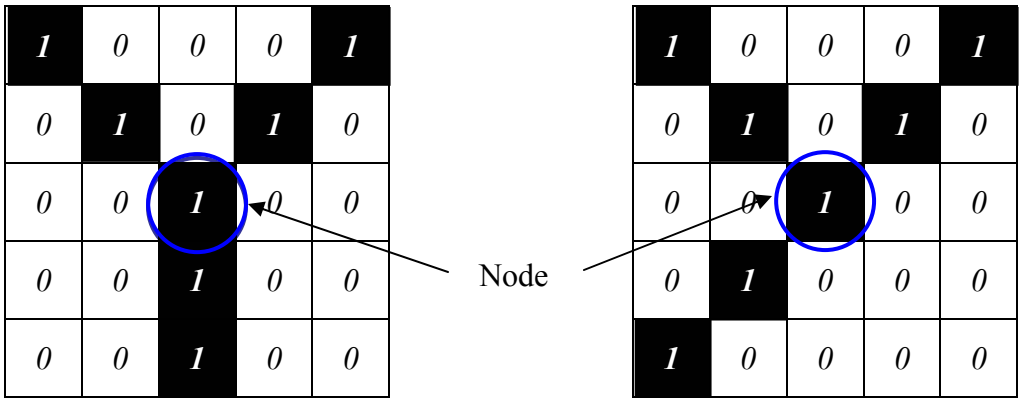

Figure 4.10. Examples of nodes.

3. If a pixel does not have any foreground neighbors in the region shown in Figure 4.10 then, that pixel is identified as the end of the fracture trace.

4. If the endpoint of the fracture trace is reached then the scanned fracture trace is saved as a separate image file. The fracture properties are calculated and saved in a text file.

4.2.5 Fracture Properties

Fracture properties such as length, orientation, width and large-scale roughness are determined from the individual fracture traces. Length is determined by summing the number of connected pixels in a fracture trace image multiplied by the size of the pixel. Pixel size is determined from the scale of the image. If the length of the fracture trace is less than a predefined length then the fracture trace is ignored. This is done to remove noise. Orientation is determined by the slope of a straight line connecting the start and end pixels of the trace map.

The width of the fracture trace is determined by returning to the threshold image. Width is the number of foreground pixels in a direction perpendicular to the fracture trace multiplied by the size of the pixel. This is illustrated in Figure 4.11.

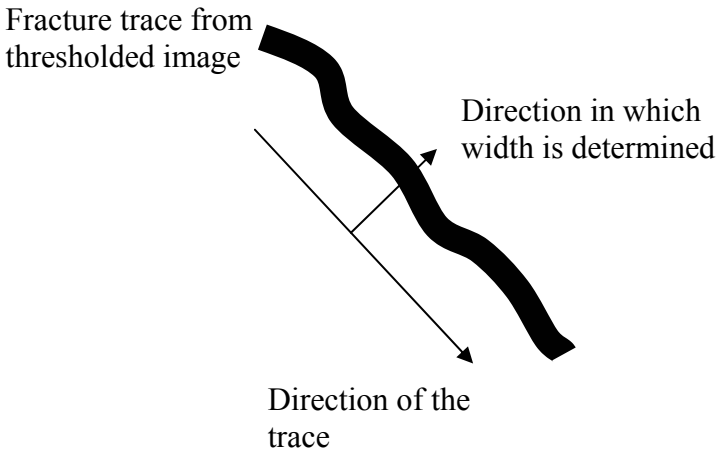

Figure 4.11. Direction in which the trace width is determined.

Large-scale average roughness is computed using a straight line connecting the two end point pixels of the trace map (baseline). The perpendicular distance from the baseline to the fracture trace is determined at random points. The average of all the distances is a measure of large scale average roughness. This is illustrated in Figure 4.12.

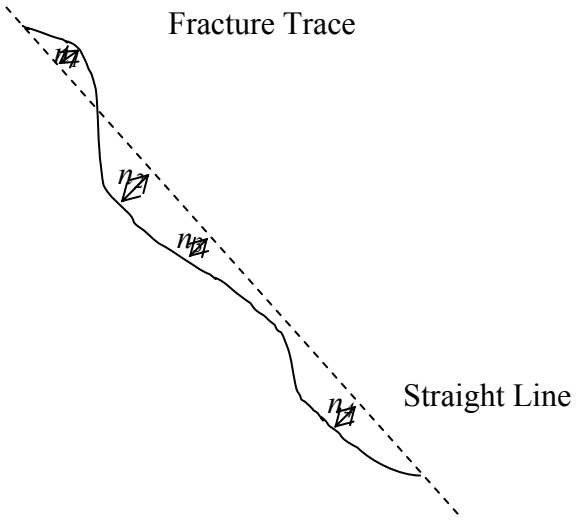

Figure 4.12. Illustration of large-scale roughness calculation.

This is quantified by the parameter Average Roughness, given by:

$$AverageRoughness = \left(\frac{n_1 + n_2 + n_3 + n_4}{4} \right). \tag{4.17}$$

In future versions of VTtrace more sophisticated roughness measures can be employed.

4.3 Programming platform and User Interface

All the image processing programs were written in Windows 2000/Windows XP platform. VTtrace and the user interface were written in Visual Basic 6.0 (VB). VB6.0 was chosen for this project since it is a widely used programming language and it is also simple and easy to work with.

A user-friendly interface is provided to execute all the image processing algorithms. Drawing and editing options like the “Pencil Tool”, “Eraser Tool” “Straight Line Tool” are provided to edit the trace map manually whenever required.

Other features provided are listed below

- Zoom in.
- Pan.
- Undo.
- Redo.
- Options to change the pencil/line thickness.

The user can select the original image file using the “open” option on the main menu. The sequence of process to extract the trace map can be done using the options provided in the main menu. Option to print the trace map or the image is also provided. Screen captures of the interface and the intermediate stages are shown in Figures 4.13 – Figure 4.17.

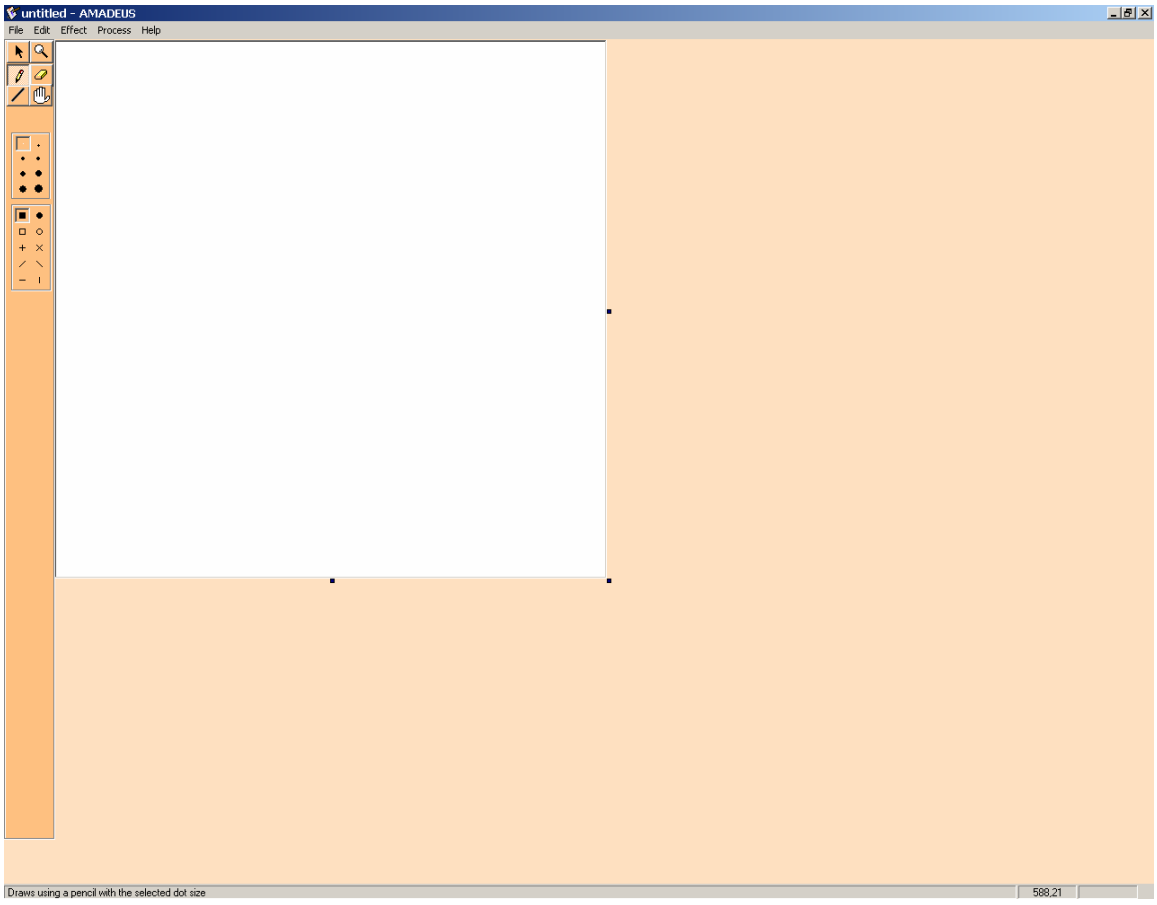

Figure 4.13 Screen capture of the user interface.

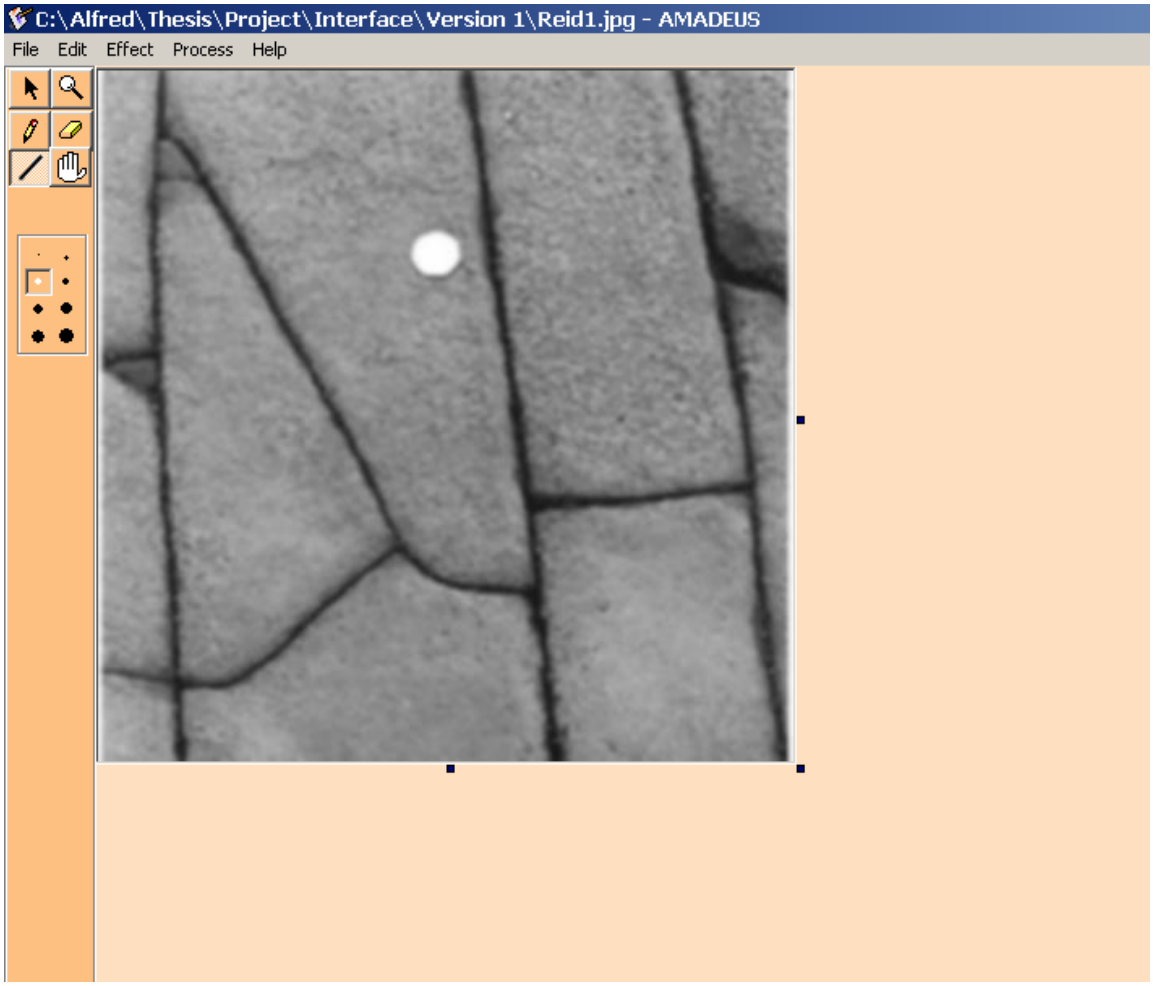

Figure 4.14. Screen Capture of the User Interface with a test image open.

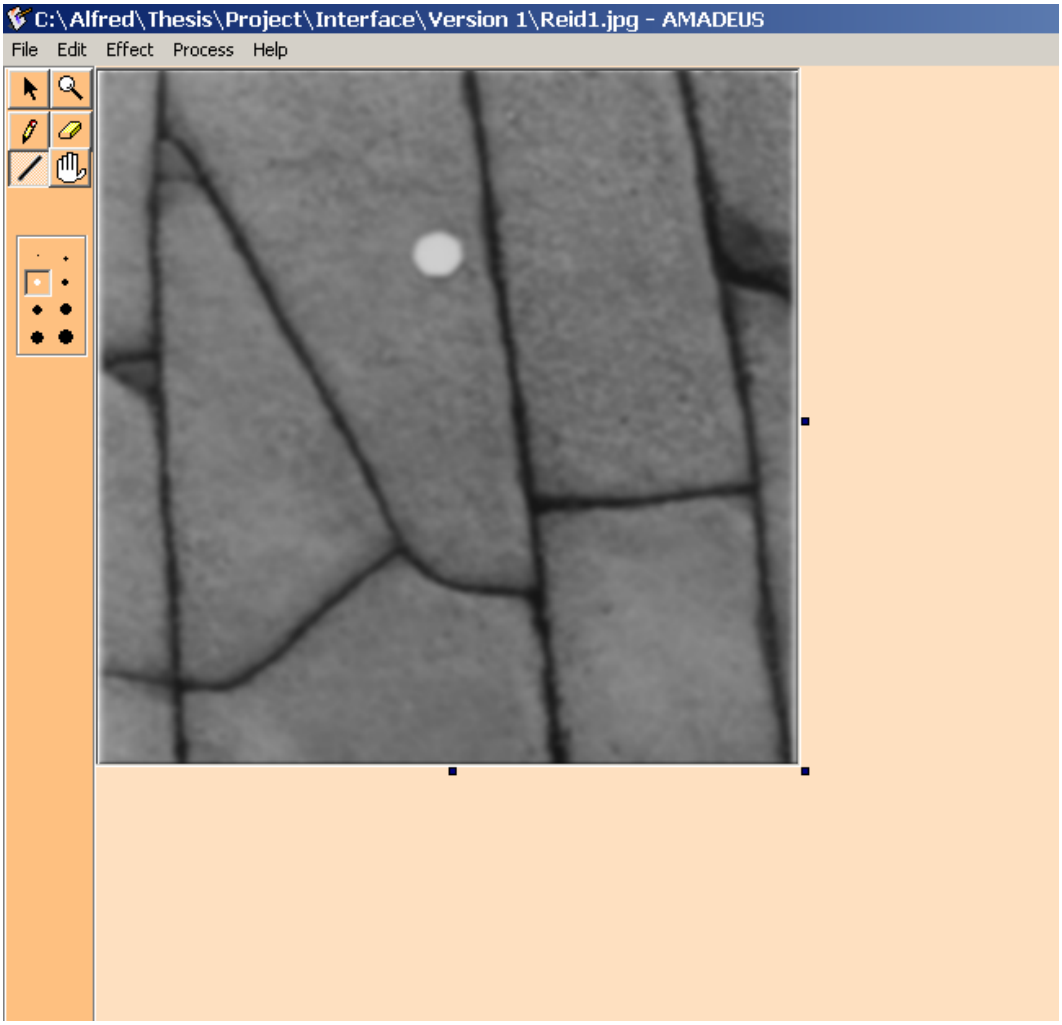

Figure 4.15. Screen Capture of the User Interface with a test image after smoothing.

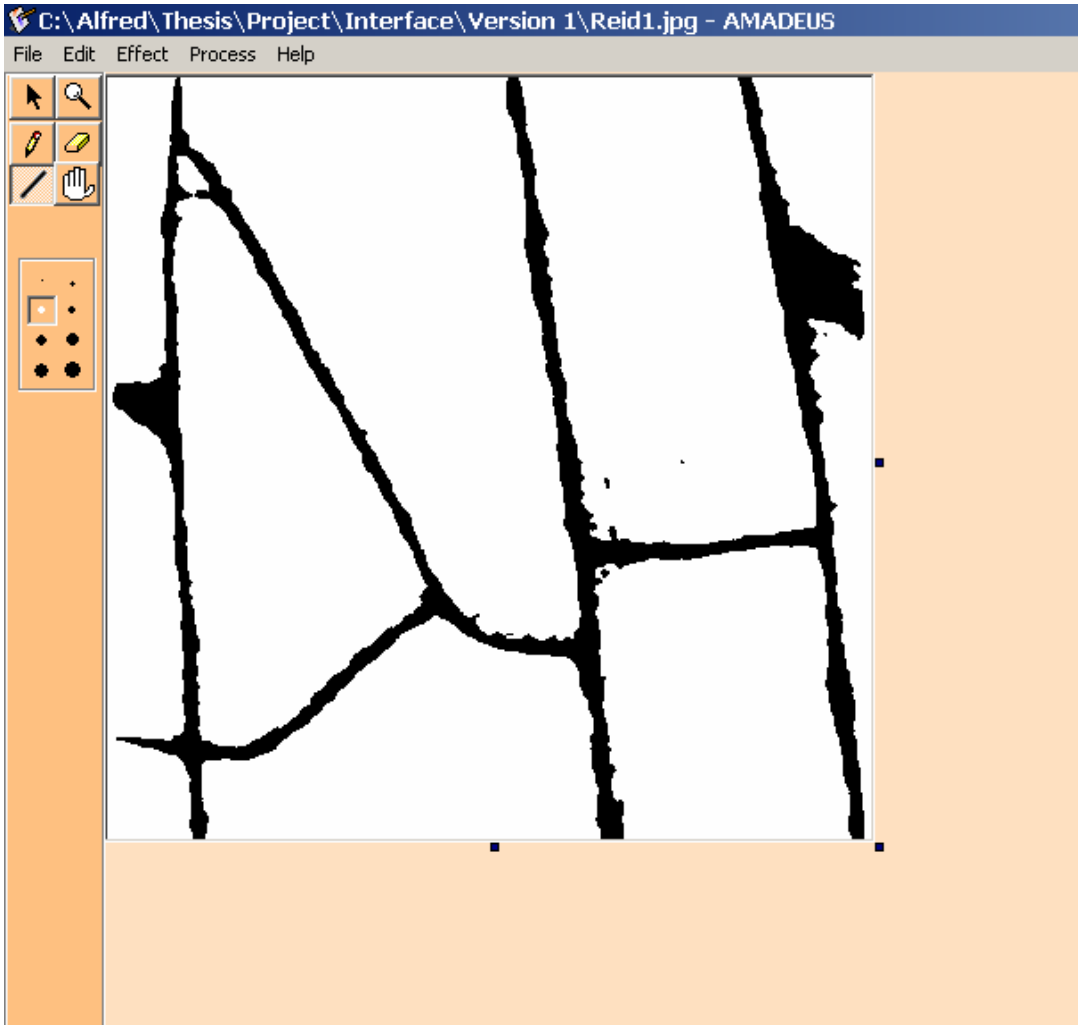

Figure 4.16 Screen Capture of the User Interface with a test image after thresholding.

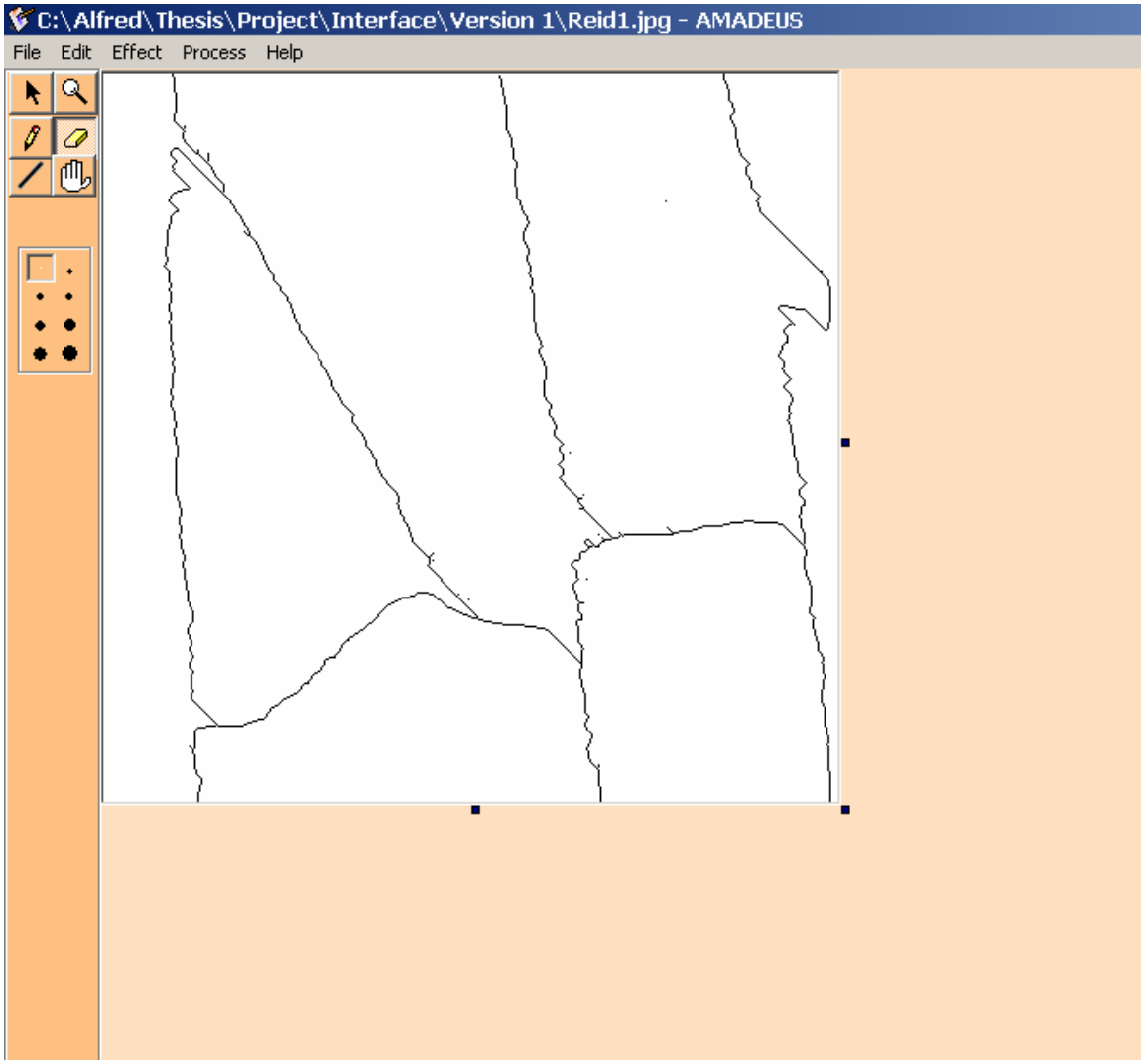

Figure 4.17 Screen Capture of the User Interface with a test image after thinning.

Chapter 5 Test Cases and Results

This chapter presents results of a series of tests conducted to evaluate each image processing algorithm and the performance of VTtrace as a whole. Each image processing algorithm was tested with both synthetic images, prepared surfaces and natural rock images. Synthetic images consisting of black lines on a white background were created using the commercial program Adobe Illustrator. Images were also made of styrofoam block discontinuity models consisting of black, hand-drawn lines on white background. Images of natural surfaces were taken in local quarries and road cuts under daylight conditions.

The user input for each stage of the individual image processing steps was varied and the corresponding results are documented. After testing the individual algorithms, the entire sequence of algorithms was executed with a set of test cases. This was done to assess usability, process cycle length and resolve any algorithm integration issues.

For ease of reading, each of the following sections is written as stand-alone discussions of each algorithm. Description of the test methodology particular to the algorithm being tested, test results and interpretation of the results are presented in each section. A critical discussion of the test results and each algorithm highlighting practical, implementation issues is included.

5.1 Image Smoothing Algorithm

Smoothing is a process to reduce the noise or distortion in the image. Various smoothing operators are available and were explained in Chapter 3. This section describes the test cases used and results of the test sequence.

5.1.1 Methodology

A 3X3 median smoothing filter (Section 4.2.1) was implemented in VTtrace since it is effective in enhancing edges and reducing noise with the least computational time. The smoothing algorithm was tested with images of rock surfaces taken in ambient, natural light conditions. The original image and the results after every pass of smoothing are presented in Figures 5.1 to Figure 5.6. Artificial “salt and pepper” noise was produced on some images and was tested for noise reduction using the smoothing

program. The images with artificial salt-pepper noise and the results are shown in Figure 5.7 to Figure 5.8.

The criteria used for evaluating the effectiveness of the algorithm include the distribution of the pixel intensity on the image and the sharpness of the edges forming the fractures.

5.1.2 Results

The results of the smoothing algorithm indicate its ability to reduce noise in the image. It can be observed from the results that the smoothing operator makes the rock surface more even and the edges are more prominent when compared to the original image. By blending the values of the matrix pixels, it will be shown in the next section that thresholding is simplified. The test on the image with the artificial salt and pepper noise illustrates the capability of the algorithm to remove distortion and dead pixels.

5.1.3 Discussion

Practical issues with the smoothing operation include preservation of small features, number of passes of the filter required, and the ability to automate the process. One problem with the smoothing operation is that some thin or small features could be lost, especially after multiple passes of the filter. Other practical problems are that the number of passes of smoothing required and the window size (e.g., 3X3 or 5X5 or 7X7) depends on the original image. The user is required to iterate using various combinations of window size and choose whichever suits that particular image best.

At this time, it is not possible to fully automate this process for images of natural surfaces in ambient light conditions. However where images are made in artificial light conditions, it may be possible to impose some degree of smoothing by controlling the intensity and type of lighting.

Figure 5.1. Original image made in natural light conditions. Note the regions with lichen growth resulting in tonal differences.

Figure 5.2. After a single pass of the 3X3 median smoothing algorithm.

Figure 5.3. After two passes of the 3X3 median smoothing algorithm.

Figure 5.4. After three passes of the 3X3 median smoothing algorithm.

Figure 5.5. After four passes of the 3X3 median smoothing algorithm.

Figure 5.6. After five passes of the 3X3 median smoothing algorithm.

Figure 5.7. Image with artificial “Salt and Pepper” noise.

Figure 5.8. Smoothed image with the “Salt and Pepper” noise removed.

5.2 Thresholding Algorithm

Thresholding is the process of converting the grayscale image to a binary (black and white) image. Due to the intensity difference between the pixels which form the fracture trace and the pixels that form the rest of the rock surface, the fractures appear as thick black lines. These lines form the basis of the fracture trace. The images are smoothened before thresholding to reduce undesired noise.

5.2.1 Methodology

For testing the performance of this algorithm, the images were converted into binary images after various levels of smoothing using different threshold values. Threshold values ranged from 150 to 50. The algorithm was also tested on images without smoothing for comparison.

5.2.2 Results

The results are presented in Figure 5.9 to Figure 5.19. It can be noticed in the results that a high threshold value picks up any small intensity difference on the surface and the width of the fracture is over represented. Low threshold value results in the breaking fractures and width of the fracture is under represented. Selecting a correct threshold value is crucial since it the basis of the fracture map and also the width of the fractures are measure from the binary image.

5.2.3 Discussion

A high threshold value will result in some undesired spots on the binary image on the other hand a low threshold value may result in some breaks on the fracture. The level on smoothing also plays an important role in this process since smoothing alters the intensity distribution in the image.

Practical problems for thresholding rock mass images include closely spaced features, noise, and lighting irregularities. If the width of the fracture is small, the thresholding operation will not detect that fracture. Also, if the fracture spacing is very close, groups of fractures may be detected as a single feature. Although at the outset this may seem a problem, it might prove to be a natural way for homogenizing the rock mass into a numerically more tractable problem.

Vegetation on the rock surfaces will require an additional step in processing to remove. However for freshly excavated faces and for underground environments, vegetation will not generally be present.

Figure 5.9. Binary image with threshold value of 150 after single pass 3X3 median smoothing.

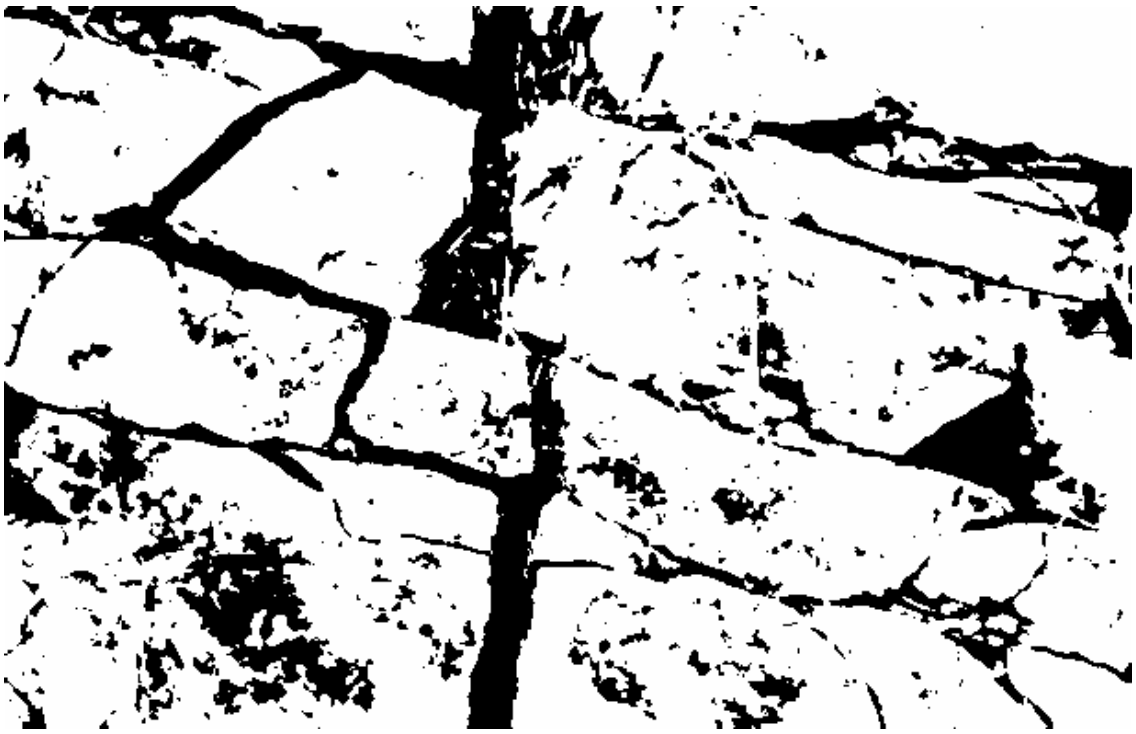

Figure 5.10. Binary image with threshold value of 128 after single pass 3X3 median smoothing.

Figure 5.11. Binary image with threshold value of 100 after single pass 3X3 median smoothing.

Figure 5.12 Binary image with threshold value of 75 after single pass 3X3 median smoothing.

Figure 5.13 Binary image with threshold value of 50 after single pass of a 3X3 median smoothing.

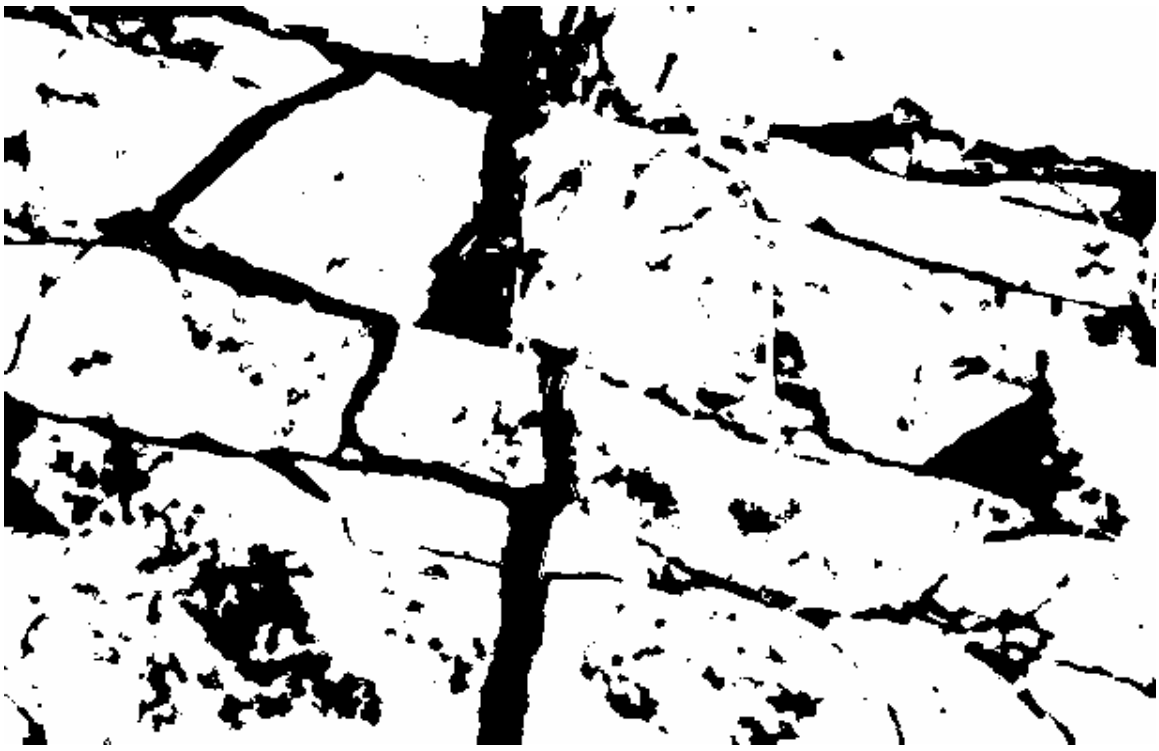

Figure 5.14 Binary image with threshold value of 128 after five pass 3X3 median smoothing.

Figure 5.15 Binary image with threshold value of 100 after five pass 3X3 median smoothing.

Figure 5.16. Binary image with threshold value of 150 without smoothing.

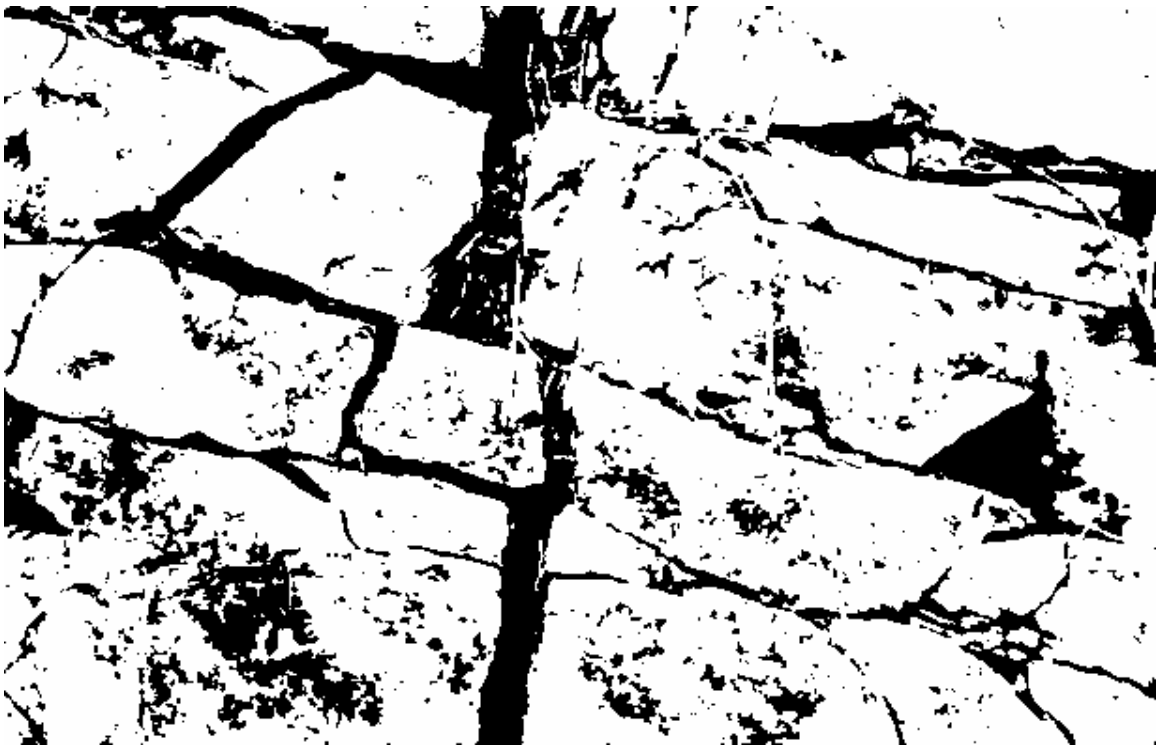

Figure 5.17. Binary image with threshold value of 128 without smoothing.

Figure 5.18. Binary image with threshold value of 100 without smoothing.

Figure 5.19. Binary image with threshold value of 50 without smoothing.

5.3 Thinning Algorithm

The binary image is thinned to extract the fracture trace map of the rock mass exposure. The outcome of the thinning process is a network of lines that are a single pixel in thickness which represent the fracture trace map.

5.3.1 Methodology

Two thinning algorithms namely the Hilditch's algorithm (Stefanelli et al., 1971) and the Zhang & Suen thinning method (Zhang et al. 1984) are provided. The user has the option to select any of the algorithms for a particular image.

Both the thinning algorithms were tested with the images after different levels of thresholding and smoothing. The effects of smoothing and thresholding can be clearly visible on the thinned image. The results of the thinning algorithm are presented from Figure 5.20 to Figure 5.31.

5.3.2 Results

The result of the thinning algorithm shows that there are some basic differences between the fracture trace maps produced by both the algorithms. Hilditch's algorithm is simple, fast and produces trace map of exactly one pixel thickness. Erosion of line segments at the end points is more severe than the Zhang & Suen algorithm. If the image has some isolated horizontal fractures, Hilditch's algorithm cannot be used since it erodes these features to a single pixel.

Objects such as a horizontal line, vertical line and a grid were created using Adobe Illustrator and were thinned using both the algorithms. The results are compared in Figures 5.32 to 5.34. The thinned images where edited using the editing options provided in the program and the final fracture trace maps are shown in Figure 5.35.

5.3.3 Discussion

The result of the thinning algorithm largely depends on the smoothing and thresholding processes since there are no user input parameters for this process. The user has the choice only to select one of the two algorithms for thinning. The results of the thinning algorithm on the images with high threshold value generates a cluster of

unwanted lines whereas the images with low threshold values generated broken traces. Hence, thresholding is the critical process that determines the quality of the trace map.

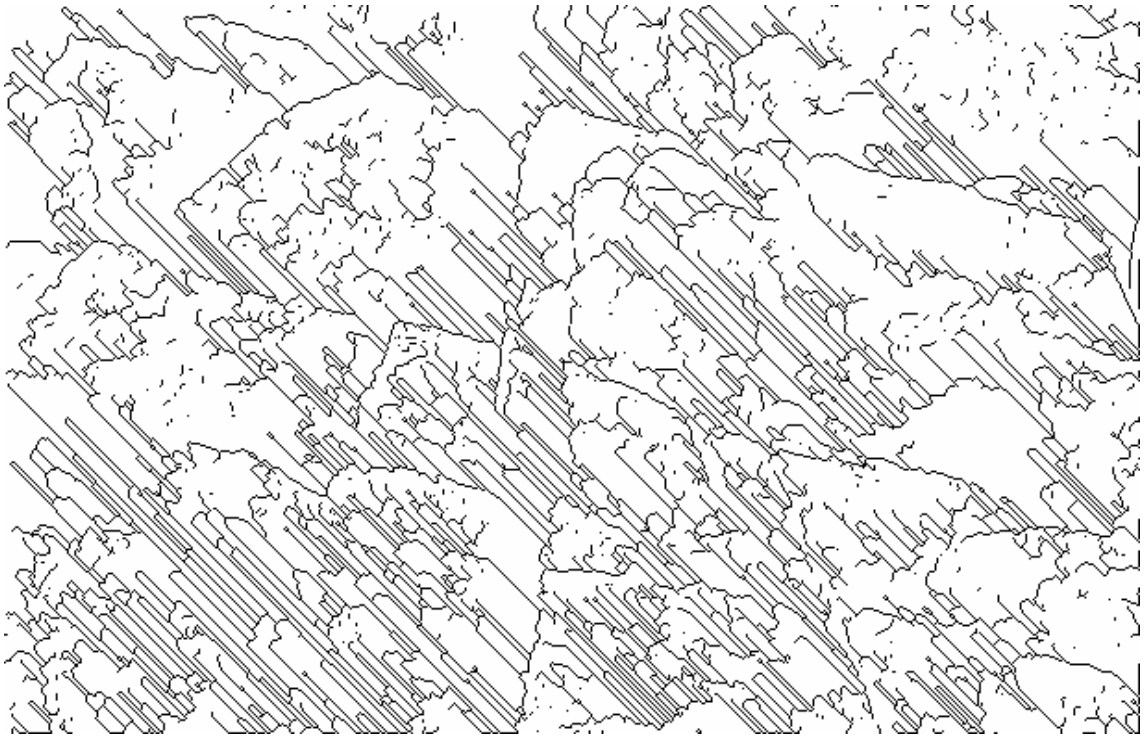

Figure 5.20. Thinned image using Hilditch's algorithm after single pass 3X3 smoothing and threshold of 150.

Figure 5.21. Thinned image using Hilditch's algorithm after single pass 3X3 smoothing and threshold of 128.

Figure 5.22. Thinned image using Hilditch's algorithm after single pass 3X3 smoothing and threshold of 100.

Figure 5.23. Thinned image using Hilditch's algorithm after single pass 3X3 smoothing and threshold of 50.

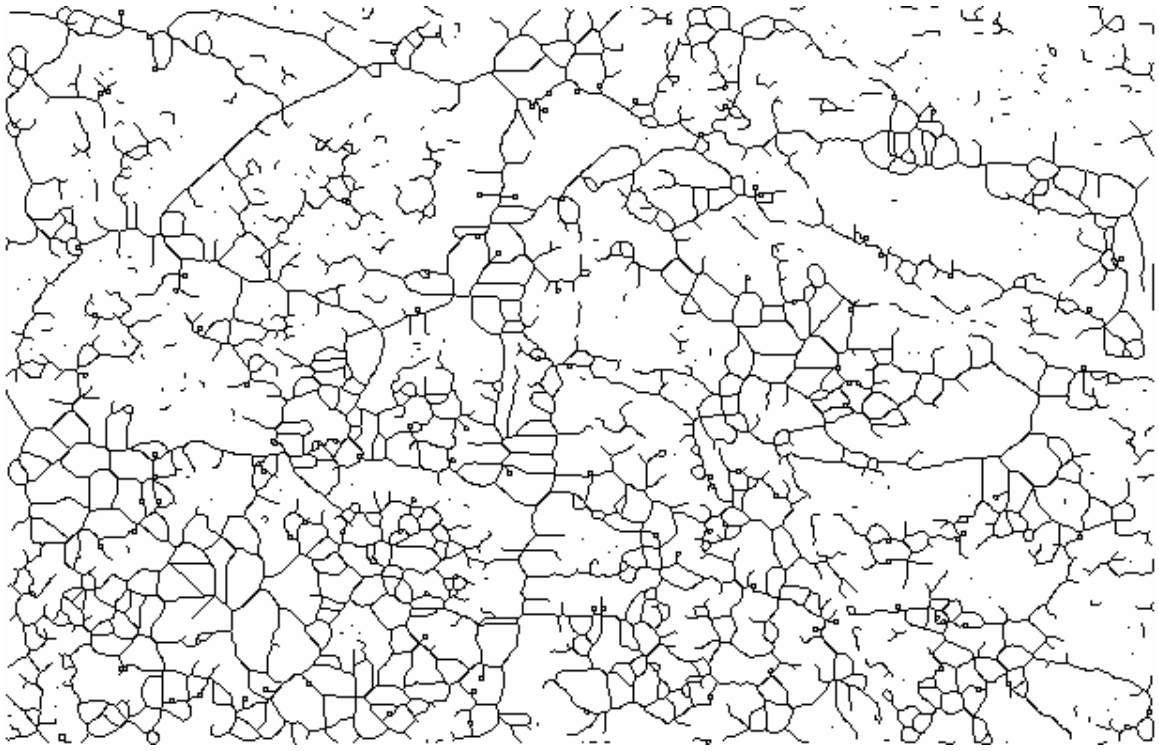

Figure 5.24. Thinned image using Zhang & Suen algorithm after single pass 3X3 smoothing and threshold of 150.

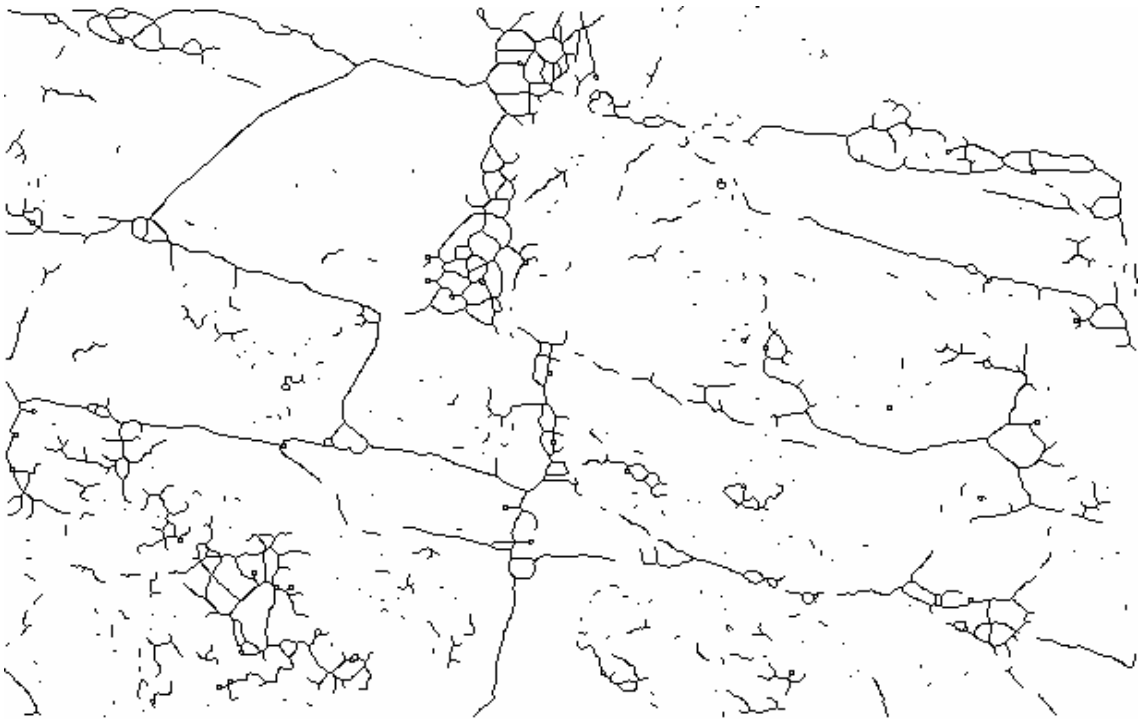

Figure 5.25. Thinned image using Zhang & Suen algorithm after single pass 3X3 smoothing and threshold of 128.

Figure 5.26. Thinned image using Zhang & Suen algorithm after single pass 3X3 smoothing and threshold of 100.

Figure 5.27. Thinned image using Zhang & Suen algorithm after single pass 3X3 smoothing and threshold of 50.

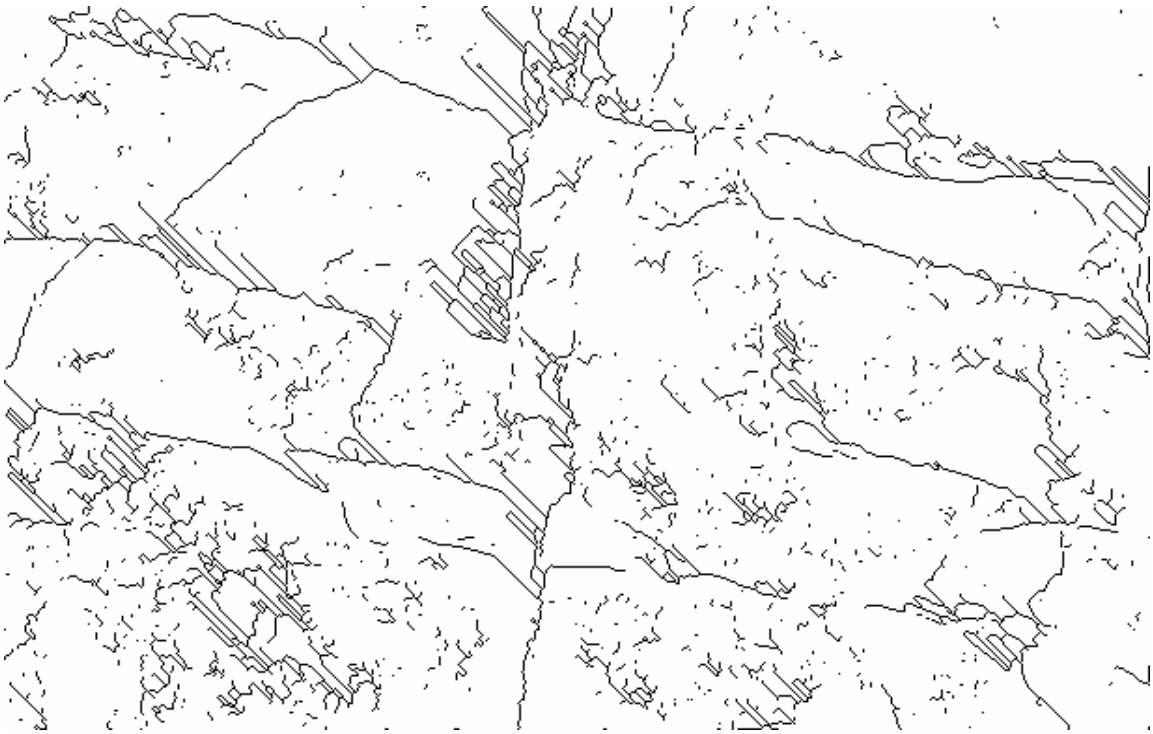

Figure 5.28. Thinned image using Hilditch's algorithm after threshold of 120 without smoothing.

Figure 5.29. Thinned image using Hilditch's algorithm after threshold of 100 without smoothing.

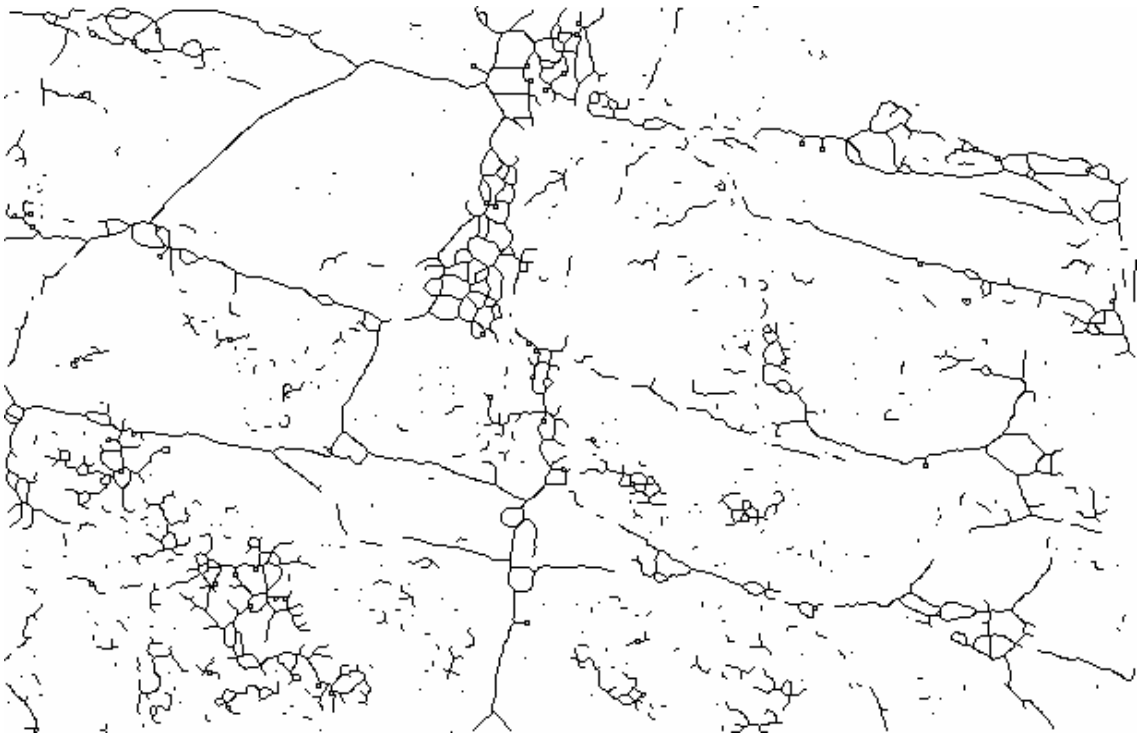

Figure 5.30. Thinned image using Zhang & Suen algorithm after threshold of 128 without smoothing.

Figure 5.31. Thinned image using Zhang & Suen algorithm after threshold of 100 without smoothing.

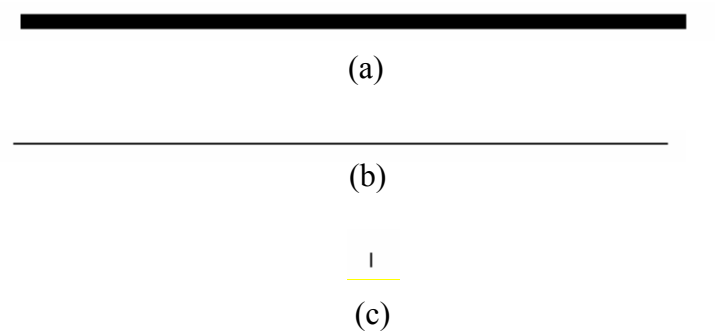

(a)

(b)

(c)

Figure 5.32. Synthetic horizontal line and results of thinning by Zhang & Suen and Hilditch's algorithms: (a) Original synthetic image, (b) original image, Zhang &Suen algorithm, (c) original image, Hilditch algorithm.

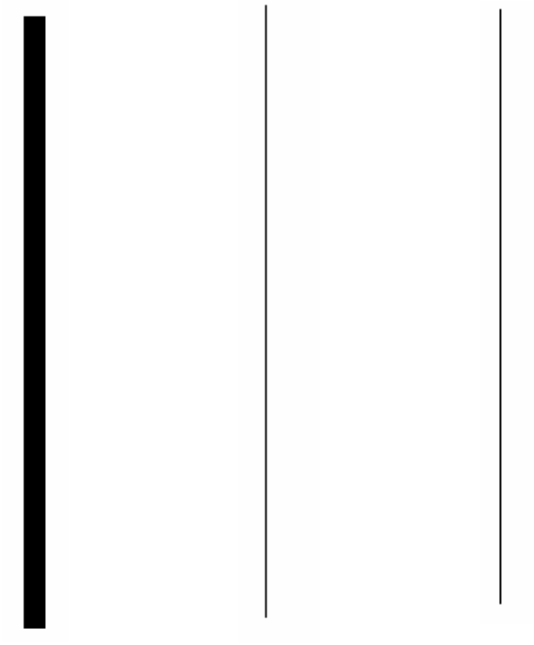

Figure 5.33. Synthetic vertical line and results of thinning by Zhang & Suen and Hilditch's algorithms: (a) Original synthetic image, (b) Zhang & Suen algorithm, (c) Hilditch algorithm.

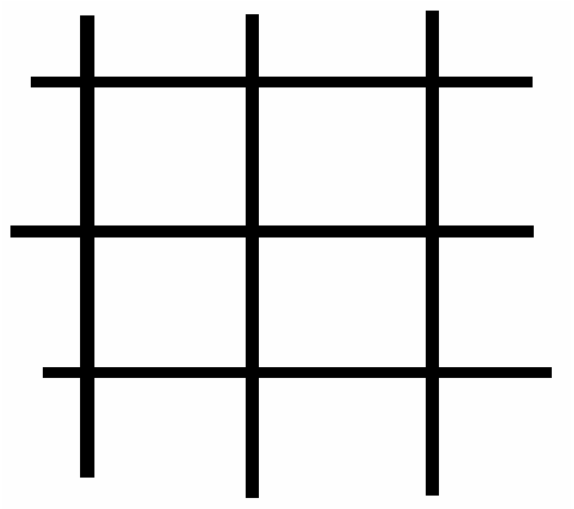

(a)

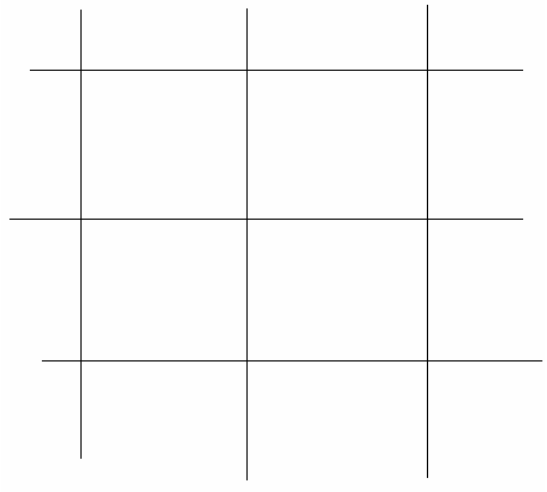

(b)

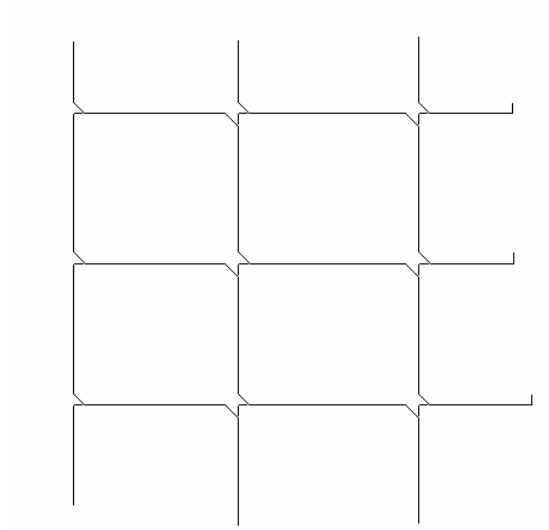

(c)

Figure 5.34 Synthetic grid pattern and results of thinning by Zhang & Suen and Hilditch's algorithms: (a) Original synthetic image, (b) Zhang & Suen algorithm, (c) Hilditch algorithm.

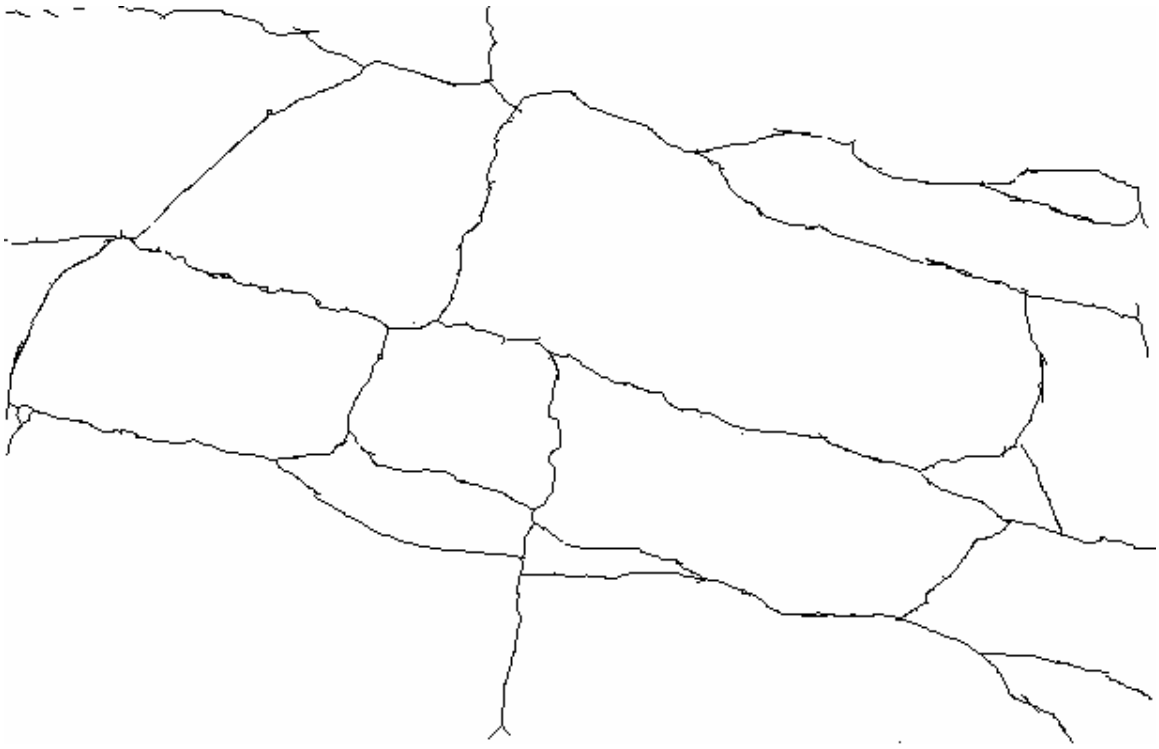

Figure 5.35. Thinned image using Zhang & Suen algorithm after single pass 3X3 smoothing and threshold at 100 after manual editing using the editing tools.

5.4 Feature characterization algorithm

The individual features are separated and stored as individual image files. The feature attributes are determined from the separated features. The final trace map after thinning and manual editing is used to obtain the feature properties such as trace length, orientation, width and large-scale roughness. Synthetic images were tested and the results are presented in Figure 5.36.

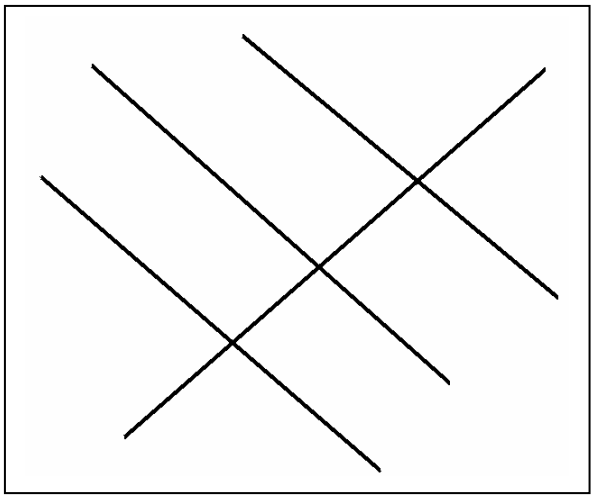

(a) Original test image before thinning

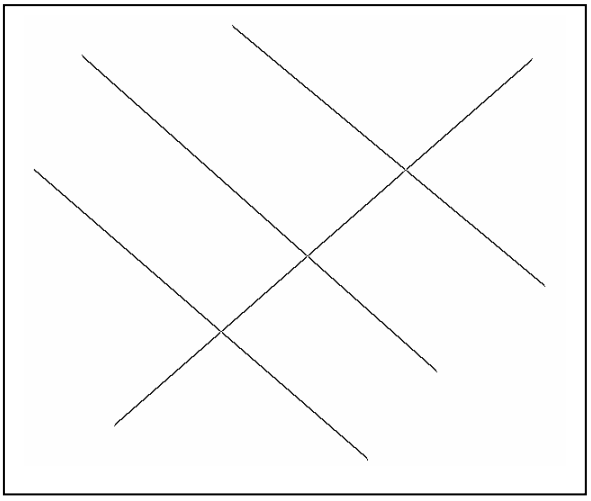

(b) Thinned test image

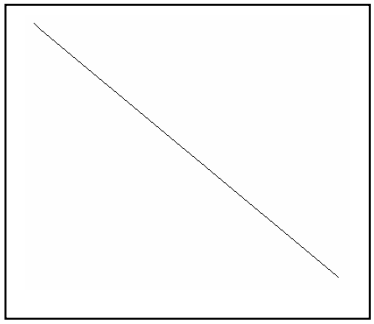

Feature Properties:
Length = 174 mm
Orientation = 39 degrees
Width = 2mm

(c) Feature 1

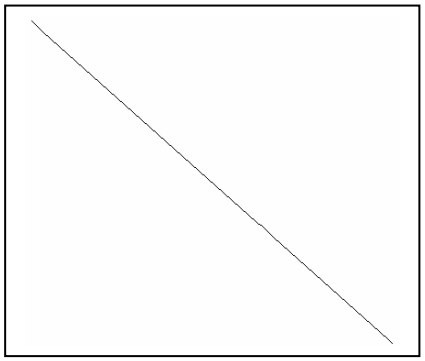

Feature Properties:
Length = 197 mm
Orientation = 42 degrees
Width = 2mm

(d) Feature 2

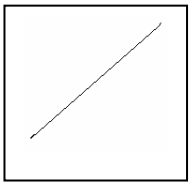

Feature Properties:
Length = 72 mm
Orientation = -41.1805 degrees
Width = 2mm

(e). Feature 3

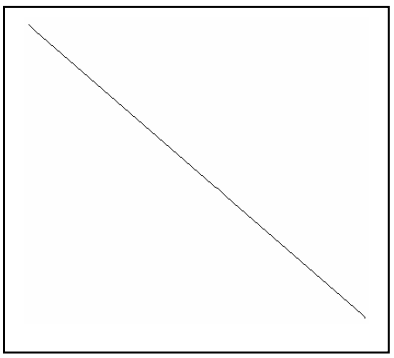

Feature Properties:
Length = 186 mm
Orientation = 41.1147 degrees
Width = 2mm

(f) Feature 4

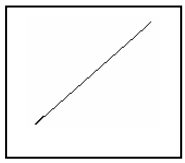

Feature Properties:
Length = 57 mm
Orientation = -40.975 degrees
Width = 2mm

(g) Feature 5

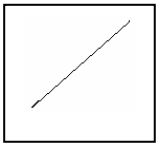

Feature Properties:
Length = 50 mm
Orientation = -41.1339 degrees
Width = 2mm

(h). Feature 6

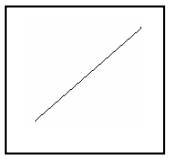

Feature Properties:
Length = 59 mm
Orientation = -41 degrees
Width = 2mm

(i) Feature 7

Figure 5.36. Original synthetic image and result of the feature characterization algorithm.

5.5 Integration Testing

The complete sequence of stages was tested with test images of rock surfaces to assess the program VTtrace as a whole.

5.5.1 Methodology

To test the complete sequence of stages, an original image of a rock surface was taken and all the algorithms were executed in sequence. Optimum parameters for each algorithm were used as determined from the trials. For thinning, Zhang & Suen's algorithm was used since it gave better results than Hilditch's algorithm. Total time taken for the entire process and the ease of use were evaluated.

5.5.2 Results

The total time taken to complete the entire sequence of steps was about 5 minutes. The thinned image was edited manually to obtain the final trace map. The time taken for manual editing is controlled by the thresholding operation since the binary image is the basis for the thinning operation. In this case, a threshold value of 100 was selected and the thinned image required less manual editing. The result of each stage is shown from Figures 5.38 to 5.42. Some of the individual fractures with their properties are shown in Figure 5.43.

5.5.3 Discussion

VTtrace is an efficient way to extract the fracture trace map. However, there are some practical problems associated with this approach that will need to be addressed in future research. Lighting plays an important role in the accuracy of the trace map since this approach utilizes the variation of light intensity levels at each pixel in the image. The image processing cannot be fully automated at this time because human intervention is required for selecting the required parameters at each stage of the process. For example, the smoothing and thresholding process are trial and error based and the user performs these operations iteratively and selects the parameter that results in the 'best' image. The parameters for the two process varies for different images depending on factors like lighting, surface texture and color, presence of vegetation and other

interferences etc. The user should also make a choice of the thinning algorithm based on which gives better results for a particular image.

Figure 5.37. Original image.

Figure 5.38. Results of single pass 3X3 median smoothing filter.

Figure 5.39. Smoothed binary image at threshold value of 100.

Figure 5.40. Result of the Zhang & Suen thinning method.

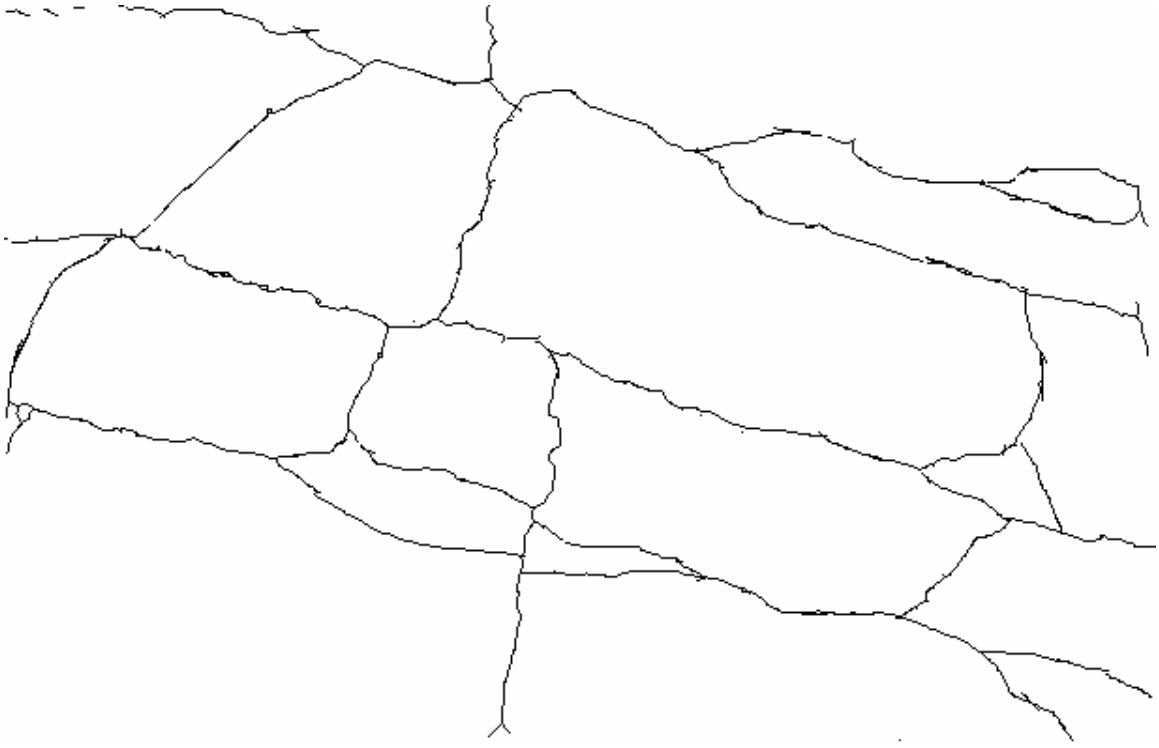

Figure 5.41. Final fracture trace map after some manual editing.

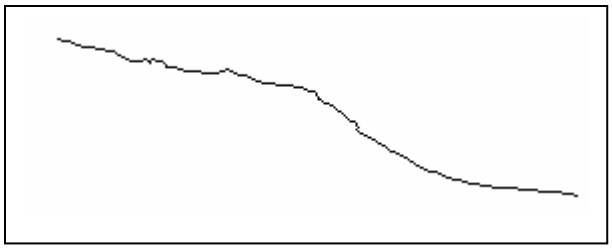

Feature Properties:
Length 65mm
Orientation 17 degrees
Width 3mm
Roughness 3mm

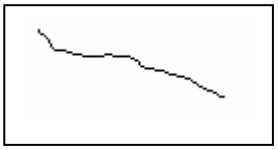

Feature Properties:
Length 12mm
Orientation 20 degrees
Width 2mm
Roughness 2mm

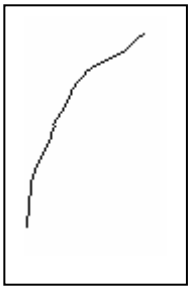

Feature Properties:
Length 26mm
Orientation -59 degrees
Width
Roughness 2mm

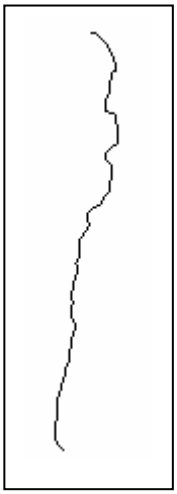

Feature Properties:
Length 55 mm
Orientation – 86 degrees
Width 4mm
Roughness 2mm

Figure 5.42. Individual features with their associated properties.

Chapter 6 Conclusions and Recommendations

VTtrace is an effective tool to aid in the solution of traditional problems in rock mechanics. The system developed as a part of this research will require some enhancement and optimization. Though the advantages of using such a system are quite obvious, it is concluded that some practical challenges remain, as listed below.

1. Lighting plays a crucial role in the accuracy of this approach. High illumination will wash out important features and low illumination will critically influence thresholding and thinning which will also lead to the loss of important information. If the system is used for underground excavations like tunneling lighting can be controlled but for outcrops the amount of sunlight and the time of the day must be considered.
2. Presence of shadows on the images can be a problem especially when the images are taken at an inclined angle, the shadows of edges tend to make the fractures thicker on the images.
3. The smoothing and thresholding operations require more than one trial with different parameters to get satisfactory results. The number of iterations required depends on the quality of image, texture and color of the rock surface, illumination, etc.
4. Erosion of the lines during thinning process may lead to the underestimation of the trace length.
5. Manual editing of the thinned image can be time consuming and laborious if large number of complex images are used.

6.1 Recommendations for Future Enhancements

Enhancements and additional features aimed at improving the efficiency and capabilities of the system are listed below.

1. Fully implement photogrammetry to obtain the feature properties in 3D space such as true trace length, width and roughness. Currently these parameters are determined in 2D image plane.
2. Optimization of the thinning algorithm to improve speed.

3. Implementation of stereo matching techniques to extract the 3D coordinates of key points on the features. This will be further used to develop the 3D model of the rock mass.
4. Converting the individual fracture traces into vector objects so that the user could pick a particular fracture trace and edit it. Currently raster editing is implemented which appears to be more time consuming than vector editing in many situations common to fracture mapping.
5. Implementation of an identification tool so that the user can pick a fracture trace and the fracture properties would be displayed.
6. Migration to VB.Net since it has better image handling capabilities that VB 6.
7. Implement procedures and algorithms for tiling and georeferencing of images for large rock exposures.
8. Creation of a database to store the fracture properties, images and any relevant information.
9. Incorporate algorithm to obtain the dip and dip direction of the fractures.
10. Implement procedures and algorithms to identify and group joint sets.

With the implementation of the above additional features and the integration of VTtrace into the AMADEUS system a significant contribution can be made in rock mechanics. Other image processing techniques like edge detection and Hough transform are some of the possible alternate solutions that might be incorporated in VTtrace. This work has significantly improved our ability to detect discontinuity traces on rock surfaces and will serve as a starting point for further research.

Chapter 7 References

Forsyth. A. D and Ponce, J. (2003). "Computer Vision A Modern Approach" Prentice Hall Inc, New Jersey; United States of America.

Gaich, A., Fasching, A., and Gruber, M. (1999). "High Resolution Stereoscopic Imaging for Tunnel Construction." Rock and Soil Engineering Nr. 1/1999.

Gaich, A., Fasching, A., and Gruber, M. (http://www.ifb.tugraz.at/situ/). "Simulation in Tunneling." Research project report.

Jain, A. K. (1989). "Fundamentals of Digital Image Processing" Prentice Hall Inc, New Jersey; United States of America.

Kemeny, J., Mofya, E., and Handy, J. (2003). "The use of Digital Imaging and laser technologies for field rock Fracture Characterization." Pan Am Conf 2003.

Klette, G. (2003). "A Comparative Discussion of Distance Transforms and Simple Deformations in Digital Image Processing." Project Report; University of Auckland; Auckland; New Zealand.

Lemy, F., and Hadjigeorgiou, J., (2003). "Rock Mass Characterization Using Image Analysis." Pan Am Conf 2003.

Lewis, R. (1990). "Practical Digital Image Processing." 1st Ed., Ellis Horwood Ltd., West Sussex, England.

Soole, P. and Poropat, G. (2000). "SIRO 3D – A 3D Imaging for Geology & Geotechnical Assessment." report for CSIRO Exploration and Mining.

Pitas, I. (2000). "Digital Image Processing Algorithms and Applications." 2nd Ed., Prentice Hall International, Great Britain.

Pratt, W. K. (2001). "Digital Image Processing" 3rd Ed., John Wiley & Sons, Inc.; United States of America.

Reid, T.R. (1998). "Methodology for the detection of discontinuity traces in digital images of rock mass exposures." PhD thesis, University of London, London, England.

Reid, T.R., and Harrison J.P., (2000). "A semi-automated methodology for discontinuity trace detection in digital images of rock mass exposures." International journal of rock Mechanics and Mining Sciences 37 (2000) 1073-1089.

Stefanelli, R and Rosenfeld, A. (1971). “Some Parallel Thinning Algorithms for Digital Pictures.” Journal of the Association for Computing Machinery, Vol. 18, No. 2, April 1971, pp. 255-264.

Zhang, T. Y., and C. Y. Suen, C. Y. (1984). “A fast thinning algorithm for thinning digital patterns.” Communications of the ACM; Vol. 27; Number 3; March 1984.